AN ABSTRACT OF THE THESIS OF

Tejas Chandrashekhar Mulky for the degree of Master of Science in Mechanical Engineering presented on September 4, 2018.

Title: Computational Study of Smoldering Combustion in Cellulose and Hemicellulose Mixtures

Abstract approved: _____

Kyle E. Niemeyer

Due to global warming wildland fires are increasing in frequency and severity. In the case of wildland fires, the major modes of combustion occur include smoldering combustion and flaming combustion. Smoldering combustion occurs most commonly in porous fuels like peat, forest duff, and woody fuels, which are available in abundance in the forest. This makes the study of smoldering combustion in these types of fuels important. Woody fuels, in general, consist of cellulose, hemicellulose, and lignin in varying proportions, and densities can also differ. However, the effects of these properties on smoldering behavior are not well understood, which motivates this investigation. In this thesis, I developed a one-dimensional computational model that can simulate smoldering combustion in cellulose and hemicellulose mixtures. I first successfully validated the model using experimental results. After validating the model, I studied the effects of varying density and fuel composition on mean peak temperature and mean propagation speed. From this study, I found that the smoldering propagation speed increases with increases in hemicellulose content, since hemicellulose pyrolyzes earlier than cellulose, resulting in faster shrinkage of the fuel and thus quicker access to oxygen for oxidation reactions. On the other hand, propagation speed decreases with increases in density, because more mass of fuel needs to be converted to char and ash, slows the fuel shrinking and slowing access to oxygen. Mean peak temperature decreases with increasing density due to higher thermal conductivity of the condensed-phase species involved, and mean peak temperature increases with hemicellulose content due to formation of lower thermal-conductivity

ash on the top, resulting in lower heat loss. I developed semi-empirical formulas for propagation speed and peak temperature capturing changes in density, mass fraction of cellulose, and mass fraction of oxygen. Next, I determined the effects of adding moisture content on peak temperatures and propagation speed for 100% cellulose, considering both expansion and lack of expansion with water addition. I found that propagation speed decreases with increasing moisture content when the fuel does not expand, due to an increase in the mass of wet fuel that needs to be dried. On the other hand, when the fuel expands on the addition of water, propagation speed decreases with additional moisture content because the fuel density decreases overall. Finally, I investigated whether the fuel composition affects the critical moisture content of ignition and extinction. I found that both critical moisture contents increase by 10% when hemicellulose content reaches 75% due to the increase in the peak temperature on the addition of hemicellulose.

Computational Study of Smoldering Combustion in Cellulose and Hemicellulose Mixtures

by

Tejas Chandrashekhar Mulky

A THESIS

submitted to

Oregon State University

in partial fulfillment of
the requirements for the
degree of

Master of Science

Presented September 4, 2018
Commencement June 2019

Master of Science thesis of Tejas Chandrashekhar Mulky presented on September 4, 2018.

APPROVED:

Major Professor, representing Mechanical Engineering

Head of the School of Mechanical, Industrial, and Manufacturing Engineering

---

Dean of the Graduate School

I understand that my thesis will become part of the permanent collection of Oregon State University libraries. My signature below authorizes release of my thesis to any reader upon request.

Tejas Chandrashekhar Mulky, Author

ACKNOWLEDGEMENTS

This work was funded by the Strategic Environmental Research and Development Program (SERDP) award RC-2651 under contract number W912HQ-16-C-0045. I would like to thank Dr. Kyle Niemeyer for advising, guiding and helping me throughout my journey as a graduate student. I would like to thank Dr. David Blunck, Benjamin Smucker, and Daniel Cowan for their helpful inputs about the topic and providing their experimental measurement data for validation. I would like to thank my committee for their time and patience in reviewing my work. I would like to thank all the members of Niemeyer Research Group who provided me with help and encouragement at crucial times. I would like to thank all the faculty whose classes I attended which helped me expand my knowledge. I would like to thank Dr. Xinyan Huang for his valuable inputs. In the end, I would like to thank my parents without their support nothing would have been possible.

TABLE OF CONTENTS

TABLE OF CONTENTS (Continued)

LIST OF FIGURES

Figure Page

LIST OF FIGURES (Continued)

Figure Page

LIST OF TABLES

Table Page

LIST OF APPENDIX FIGURES

LIST OF APPENDIX TABLES

Chapter 1: Introduction

Natural and human-caused wildland fires destroy infrastructure and natural resources, and in the worst case can cause loss of human life in affected areas, particularly at wildland–urban interfaces. The overall socioeconomic loss due to wildland fire is extremely large. Power et al. [4] found that the number of wildland fires globally has been monotonically increasing over the last 21,000 years.[1] This increasing trend in wildland fires is attributed to climate change since global warming is causing forests and biomass to dry, which in turn increases the frequency of occurrence and severity of fires [6]. Wildland fires also have a huge impact on the environment. Raupach et al. [7] found that total CO_2 emissions from wildland fires contribute to 26–31 % of the total CO_2 emissions coming from fossil fuels. This means wildland fires are a major contributor to global climate change, placing them in a vicious circle of feedback.

The two major combustion processes that occur in fire are flaming combustion and smoldering combustion [8]. Flaming and smoldering involve different chemical processes and hence show different characteristics. Flaming combustion involves rapid gas-phase oxidation reactions [9]. So, sustaining flaming combustion requires fuel from pyrolysis in the volatile state. Smoldering combustion, on the other hand, involves slow char-oxidation reactions, so once char starts accumulating on the surface of the fuel through pyrolysis, the diffusing oxygen on the surface of the fuel sustains smoldering combustion [8]. Both of these types of combustion are hazardous in their own ways. However, smoldering combustion has not been studied to the same extent as flaming combustion [10]. Smoldering combustion in some ways can be more hazardous compared to flaming combustion. Smoldering combustion has lower combustion efficiency compared to flaming combustion [8], because the lower temperatures of smoldering leads to incomplete oxidation, resulting in emissions of more CO and other pollutants. Smoldering combustion is also difficult to suppress compared with flaming combustion because in general smoldering can be sustained at lower oxygen concentrations and requires more water to extinguish (and

[1] However, over the last 30 years in the U.S., the number of wildfires has remained constant while the total acres burned has nearly quadrupled [5].

may be underground) [9]. Smoldering can also easily transition back to flaming combustion. As a result of these characteristics, smoldering fires are some of the largest and most influential fires in the world, which has motivated increased study into smoldering combustion.

Smoldering combustion occurs most commonly in porous fuels since oxygen can diffuse easily into such fuels. Fuels abundantly available in forests and wildlands, which are at risk of wildfires, include forest duff, peat, and other woody fuels. These fuels are porous in nature and thus prone to smoldering combustion. Such fuels are generally made up of cellulose, hemicellulose, and lignin in varying proportions [1, 11]. The chemical composition of fuels impacts their smoldering characteristics: spread rate of smoldering varies from fuel to fuel. For example, cotton is mainly composed of cellulose, and smoldering propagation speed in cotton varies 2–4 mm/min in the density range 5–100 kg/m^3 [12]. In contrast, smoldering in peat—a complex lignocellulosic biomass, i.e., a composite of cellulose, hemicellulose, and lignin—propagates at speeds of 0.083–0.333 mm/min for densities of 130–180 kg/m^3 [13]. The significant difference in smoldering propagation between these fuels indicates its dependence on fuel composition and density. In addition, most fuels have some natural moisture content, which also affects smoldering combustion [13, 14].

The importance of smoldering combustion to wildfire behavior and emissions combined with the dependence of smoldering behavior on fuel characteristics motivates a detailed study to understand the effects of varying density, fuel composition, and moisture content on smoldering propagation speed and peak temperature. This information will be useful for fire managers to estimate how far and fast a fire may propagate, which may be crucial information to extinguish smoldering combustion by digging a fire-break trench to isolate the affected area. Also, it will help estimate how much organic matter may have been destroyed by smoldering combustion. Developing a predictive smoldering model can also improve existing large-scale fire models that involve competition between smoldering and flaming combustion.

1.1 Objectives

The overall goal of my research is to understand how downward propagating smoldering behavior changes when fuel composition, fuel density, and moisture content is varied in

a cellulose and hemicellulose mixtures. This thesis focuses on mixtures of cellulose and hemicellulose as a first step to fully understanding smoldering in general lignocellulosic biomass, with the following objectives:

- Develop a one-dimensional model that can simulate downward propagation of smoldering combustion in cellulose and hemicellulose mixtures and validate it against experimental results;
- Investigate how and why varying density affects smoldering combustion;
- Determine the affect of varying fuel composition on smoldering combustion and explain why do we see the observed trends;
- Examine how moisture content impacts differently smoldering in fuels which expands on addition of water similar to peat and which doesn't;
- Identify whether fuel composition affects the critical moisture content of ignition and extinction.

1.2 Outline

Chapter 2 contains a peer-reviewed article published in the *Proceeding of the Combustion Institute* (in press, 2019). In this manuscript, I developed a one-dimensional computational model for cellulose and hemicellulose mixtures and validated it against experimental measurements taken by collaborators. I performed a preliminary analysis into the effects of density, fuel composition, and moisture content on smoldering combustion and hypothesized possible reasons for the observed trends. Chapter 3 contains a manuscript, intended for submission to peer-reviewed journal, that builds on the first manuscript by updating the computational model. I validated this updated model against a different experimental setup where the experiments were carried out in one-dimensional reactor box that better matches the modeled configuration and boundary conditions. Using the updated model, I performed an in-depth analysis of the effect of density and fuel composition on smoldering combustion. I studied the relationship between oxygen concentration, density, and propagation speed and developed a semi-empirical formula for smoldering propagation speed. Then, I examined how moisture content affects smoldering combustion in these fuel mixtures, including looking at the effect of fuel expansion with the

addition of water. Finally, I determined whether critical moisture content of ignition and extinction depends on fuel composition. Chapter 4 summarizes the findings of my thesis and presents directions for future work.

Computational study of the effects of density, fuel content, and moisture content on smoldering propagation of cellulose and hemicellulose mixtures

Tejas Chandrashekhar Mulky and Kyle E. Niemeyer

Proceedings of the Combustion Institute, in press, 2019.
https://doi.org/10.1016/j.proci.2018.06.164

Chapter 2: Computational study of the effects of density, fuel content, and moisture content on smoldering propagation of cellulose and hemicellulose mixtures

Abstract

Smoldering combustion plays an important role in forest and wildland fires. Fires from smoldering combustion can last for long periods of time, emit more pollutants, and be difficult to extinguish. This makes the study of smoldering in woody fuels and forest duff important. Cellulose, hemicellulose, and lignin are the major constituents in these type of fuels, in different proportions for different fuels. In this paper, we developed a 1-D model using the open-source software Gpyro to study the smoldering combustion of cellulose and hemicellulose mixtures. We first validated our simulations against experimentally obtained values of propagation speed for mixtures with fuel compositions including 100%, 75%, 50%, and 25% cellulose, with the remaining proportion of hemicellulose. Then, we studied the effects of varying fuel composition, density, and moisture content on smoldering combustion. We find that propagation speed of smoldering increased with decreases in density and increases in hemicellulose content, which we attribute to the role of oxygen diffusion. Propagation speed increased with moisture content for pure cellulose up to a certain limiting value, after which the propagation speed dropped by up to 70%. The mean peak temperature of smoldering increased with increases in hemicellulose content and density, and decreased with increasing moisture content.

2.1 Introduction

Smoldering is a flameless, slow, and low-temperature form of combustion. It is considered to be a major fire hazard, because compared with flaming combustion it can persist for long periods of time and is difficult to suppress [9]. The wildfires in Rothiemurchus, Scotland, that occurred during July 2006 exemplify these characteristics: the flaming part of the fire was extinguished within three days while smoldering lasted for more than

40 days—even through rain [10]. Smoldering combustion also produces large amounts of greenhouse gases since it operates at lower temperatures resulting in incomplete oxidation. In 1997, Indonesia's forest fires contributed around 13–40% of the total greenhouse gases emitted by fossil fuels that year [15].

Smoldering combustion can self-sustain in fuels that form char when heated since char oxidation is the main source of heat for smoldering combustion in many cases [9, 16, 17]. This makes study of smoldering combustion important in fuels like peat, forest duff, and woody fuels because of their abundant presence in forest. Such type of fuels are primarily made up of cellulose, hemicellulose, and lignin in varying proportions [1, 11, 18], where each constituent plays a role in the pyrolysis and combustion process [1, 11]. Smoldering combustion is generally represented by pyrolysis and oxidation reactions [9]. Some studies have looked into the contributions of these constituents to pyrolysis. Gani [19] found that samples with more cellulose content pyrolyzed faster than samples with more lignin. However, we are unaware of any studies that examined how changes in fuel composition affect smoldering combustion. These fuels also have different amounts of moisture content (MC), depending upon the porosity of the fuel and weather conditions. Peat, for example, can have MC ranging from 10 to 300% depending on the weather conditions in a given region [14]. Huang and Rein [13] recently showed that downward propagation speed of smoldering increases with increasing moisture content for peat both experimentally and computationally for a range of moisture content from 0 to 70%. They attributed this increase in spread rate to enhancement of thermal conductivity and reduction in the density of fuel due to addition of water [13].

In this paper, we study smoldering combustion in cellulose and hemicellulose mixtures. We developed a one-dimensional computational model for a reactive, porous medium with the open-source software Gpyro. We first validate the model against experimental values of propagation speed and mean peak temperature. Then, we look at how changes in fuel composition, density, and moisture content affect the smoldering propagation speed and mean peak temperature. Wildlands and forests have abundant duff and woody fuels with varying fuel composition, fuel density, and moisture content. Understanding how these properties affect smoldering characteristics will help improve understanding of smoldering in wildland/forest fires and help inform large-scale models used—and decisions made—by land managers.

2.2 Computational model

In this article, we investigate the downward propagation of smoldering. Hence, we developed a one-dimensional computational model with a computational domain of 0.0875 m. This domain size was chosen to match that of the experiment against which we will validate our model, where fuel was loaded in a container with the dimensions $0.2 \times 0.2 \times 0.0875\,\mathrm{m}^3$; Cowan et al. [20] provide additional details on the experimental configuration. Additional information about the experiment is provided in the supplementary material. The top surface was open to the atmosphere while the bottom surface was insulated.

In this model, the condensed phase and gas phase are assumed to be in thermal equilibrium (i.e., they have the same temperature). (Not making this assumption changes the calculated propagation speeds within 5.6%, but at a greater computational expense.) The shrinkage of the sample during the smoldering process is taken into consideration by decreasing cell heights (Δz) [21]. The Schmidt number is taken as unity. All the simulations were run with an initial time-step size of 0.02 s and uniform cell size of 10^{-4} m. These values were selected after performing a grid refinement study by reducing the spatial and initial time step by a factor of two, which only changed propagation speeds by 1.23%. We provide a more detailed grid convergence study in the supplementary material.

2.2.1 Governing equations

We developed the one-dimensional model using the open-source software Gpyro [21, 22], which solves 1D transient conservation equations for condensed-phase mass Eq. (2.1), gas-phase mass Eq. (2.2), condensed-phase species Eq. (2.3), gas-phase species Eq. (2.4), condensed-phase energy Eq. (2.5), and gas-phase momentum Eq. (2.6), shown below; the ideal gas law Eq. (2.7) closes the set of equations. Gpyro is also capable of doing 2D and 3D simulations. Lautenberger and Fernandez-Pello [21] provide more details about these governing equations and how Gpyro solves them numerically.

$$\frac{\partial \overline{\rho}}{\partial t} = -\dot{\omega}'''_{fg}\,, \tag{2.1}$$

$$\frac{\partial (\rho_g \overline{\psi})}{\partial t} + \frac{\partial \dot{m}''}{\partial z} = \dot{\omega}'''_{fg}\,, \tag{2.2}$$

$$\frac{\partial (\overline{\rho} Y_i)}{\partial t} = \dot{\omega}'''_{fi} - \dot{\omega}'''_{di}\,, \tag{2.3}$$

$$\frac{\partial(\rho_g \overline{\psi} Y_j)}{\partial t} + \frac{\partial(\dot{m}'' Y_j)}{\partial z} = -\frac{\partial}{\partial z}(\overline{\psi}\rho_g D \frac{\partial Y_j}{\partial z}) + \dot{\omega}'''_{fj} - \dot{\omega}'''_{dj} \,, \tag{2.4}$$

$$\frac{\partial(\overline{\rho}\overline{h})}{\partial t} = \frac{\partial}{\partial z}(\overline{k}\frac{\partial T}{\partial z}) - \dot{Q}'''_{s-g} + \sum_{k=1}^{K} \dot{Q}'''_{s,k} - \frac{\partial \dot{q}''_r}{\partial z} + \sum_{i=1}^{M}((\dot{\omega}'''_{fi} - \dot{\omega}'''_{di})h_i) \,, \text{ and} \tag{2.5}$$

$$\dot{m}'' = -\frac{\overline{K}}{v}\frac{\partial P}{\partial z} \,, \tag{2.6}$$

$$P\overline{M} = \rho_g R T_g \,, \tag{2.7}$$

where ρ is the density, M is the number of condensed-phase species; X is the volume fraction; $\dot{\omega}'''$ is the reaction rate; Y_j is the jth species mass fraction; ψ is the porosity; K is the permeability/number of reactions; $\overline{M}$ is the mean molecular mass obtained from local volume fractions of all gaseous species; $\dot{q}''_r$ is the radiative heat-flux; $\dot{Q}'''$ is the volumetric rate of heat release/absorption; R is the universal gas constant; D is the diffusion coefficient; h is the enthalpy; P is the pressure; subscripts f, d, i, j, k, s, and g are formation, destruction, condensed-phase species index, gas-phase species index, reaction index, solid, and gas. The overbar over ρ, ψ, K, k indicates an averaged value weighted by condensed-phase volume fraction, while the overbar over h indicates averaged value weighted by condensed-phase mass fraction.

2.2.2 Boundary conditions

The ambient pressure (P_∞) and temperature (T_∞) were set to 1 atm and 293 K, respectively. The top surface was modeled as open to atmosphere. For all simulations, pressure at the top surface ($z = 0$ m) is set equal to the ambient pressure, Eq. (2.12). The convective heat transfer coefficient at $z = 0$ m is set as $h_{c0} = 1.52\Delta T^{1/3} \approx 10\,\mathrm{W/m^2K}$, which takes into account cooling by the atmosphere at top surface [1], and the mass transfer coefficient (h_{m0}) is set at 0.01 [14]. The mass fractions of oxygen ($Y_{\infty,\mathrm{O_2}}$) and nitrogen ($Y_{\infty,\mathrm{N_2}}$) were fixed at 0.23 and 0.77, respectively. The emissivity (ϵ) is set at 0.95.

To validate the model using experimental results, we specified the boundary condition at the top surface ($z = 0$ m) by setting the temperature as equal to the experimentally

obtained values (via thermocouple) $T_{\text{exp}}(t)$ at $z = 0\,\text{m}$, using Eq. (2.8):

$$T|_{z=0}(t) = T_{\text{exp}}(t)\ . \tag{2.8}$$

Since the thermocouple at $z = 0\,\text{m}$ does not move as the fuel shrinks, we modeled our boundary condition to behave in the same way (i.e., remaining applied at $z = 0$.

For our remaining studies, we studied the effect of density and moisture content on smoldering. For those cases, we specified the boundary condition at top surface by applying a heat flux ($\dot{q}_e''$) represented by Eq. (2.9). Once the sample is successfully ignited, for the rest of the simulation we applied a convective–radiative heat balance to the top surface, represented by Eq. (2.10):

$$-\overline{k}\frac{\partial T}{\partial z}\bigg|_{z=0} = -h_{c0}(T_{z=0} - T_\infty) + \overline{\epsilon}\dot{q}_e'' - \overline{\epsilon}\sigma(T_{z=0}^4 - T_\infty^4)] \quad \text{and} \tag{2.9}$$

$$-\overline{k}\frac{\partial T}{\partial z}\bigg|_{z=0} = -h_{c0}(T_{z=0} - T_\infty) - \overline{\epsilon}\sigma(T_{z=0}^4 - T_\infty^4)\ . \tag{2.10}$$

Additional boundary conditions at the top surface include

$$-\left(\overline{\psi}\rho_g D\frac{\partial Y_j}{\partial z}\right)\bigg|_{z=0} = h_{m0}\left(Y_{j\infty} - Y_j|_{z=0}\right) \quad \text{and} \tag{2.11}$$

$$P|_{z=0} = P_\infty\ . \tag{2.12}$$

For all cases, we modeled the bottom surface as insulated. The convective heat transfer coefficient (h_{cL}) at the bottom surface was set at $3\,\text{W/m}^2\text{K}$ [14]. This takes into account the small amount of heat transfer across the insulated wall. The mass transfer coefficient (h_{mL}) and mass flux (m_L'') were both set at 0. The additional equations used for the boundary conditions at the bottom surface are

$$-\overline{k}\frac{\partial T}{\partial z}\bigg|_{z=L} = -h_{cL}(T|_{z=L} - T_\infty)\ , \tag{2.13}$$

$$-(\overline{\psi}\rho_g D\frac{\partial Y_j}{\partial z})\bigg|_{z=L} = h_{mL}(Y_{j\infty} - Y_j|_{z=L})\ , \text{ and} \tag{2.14}$$

$$\dot{m}''|_{z=L} = 0\ . \tag{2.15}$$

2.2.3 Physical properties

The kinetic model used in this work includes five condensed-phase species: cellulose, hemicellulose, alpha-char, beta-char, and ash. The model of Huang et al. [1] produces two types of char from the fuel: α-char and β-char. The α-char is obtained from cellulose pyrolysis while β-char is obtained from oxidative degradation of cellulose, but we assumed the properties of α-char and β-char to be the same [1]. For validation, the bulk density of cellulose and hemicellulose were measured experimentally [20]. The bulk density of char and ash were calculated using the relations $\rho_{\text{char}} \approx 0.25 \times \rho_{\text{cellulose}}$ [13] and $\rho_{\text{ash}} \approx \text{IC}/100 \times 10 \times \rho_{\text{cellulose}}$, where IC stands for inorganic content [23]. The IC for cellulose and hemicellulose is taken as 0.3% and 1.7% respectively [3]. The bulk density of the mixture in this model (ρ_{mix}) is calculated by taking into account the bulk density of cellulose and hemicellulose before mixing and mass fraction of those species (Y_i) in the mixture:

$$\rho_{\text{mix}} = \left(\frac{Y_{\text{cellulose}}}{\rho_{\text{cellulose}}} + \frac{Y_{\text{hemicellulose}}}{\rho_{\text{hemicellulose}}} \right)^{-1} . \tag{2.16}$$

Table 2.1 provides other physical properties of the condensed-phase species, which includes solid density (ρ_s), thermal conductivity (k), and heat capacity (c_p).

Table 2.1: Thermophysical properties of condensed phase species

Species	Solid density (kg/m^3)	Thermal conductivity (W/(m K))	Heat capacity (J/(kg K))	Source
Cellulose	1500	0.356	1674	[24]
Hemicellulose	1365	0.34	1200	[25–27]
Char	1300	0.26	1260	[1, 28]
Ash	2500	1.2	880	[1, 28]

Porosity (ψ_i) and effective thermal conductivity (k_i) are calculated using $\psi_i = 1 - (\rho_i/\rho_{s,i})$ and $k_i = k_{s,i}(1-\psi_i)+\gamma_i \sigma T^3$, respectively, where γ is the parameter controlling the radiation heat transfer across pores [1, 21, 29]. The pore diameter (d_p), permeability (K), and the parameter controlling the radiation heat transfer across pores (γ) are calculated using equations (2.17), (2.18), and (2.19), respectively, which were obtained from [1, 29,

30]:

$$d_{p,i} = \frac{1}{S_i \times \rho} \tag{2.17}$$

$$K \approx 10^{-3} \times d_{p,i}^2 \tag{2.18}$$

$$\gamma_i \approx 3 \times d_{p,i} \ , \tag{2.19}$$

where S is the particle surface area. The particle surface areas of fuel and char are assumed to be the same [14]. The values of particle surface area of cellulose, ash obtained from cellulose, hemicellulose, and ash obtained from hemicellulose are 0.024, 0.096, 0.0678, and 0.2712 m^2/g, respectively [1, 31, 32]. For simulations with moisture content, the natural expansion process during water absorption is taken into account. To account for this process, we applied a correlation to calculate the dry bulk density (ρ_{dc}) and wet bulk density (ρ_{wc}): $\rho_{dc} = (170 + 40MC)/(1 + MC)$ and $\rho_{wc} = (170 + 40MC) = \rho_{dc}(1 + MC)$, respectively [13]. This correlation was developed for peat, which has a porosity of around 0.91, close to that of cellulose at 0.88; in contrast, the porosity of hemicellulose is around 0.53. Thus, we only used this correlation for fuels with 100% cellulose.

2.2.4 Chemical kinetics

The reaction rate is expressed using Arrhenius kinetics:

$$\dot{\omega}'''_{dA_k} = Z_k \frac{(\overline{\rho} Y_{A_k} \Delta z)_{\sum}}{\Delta z} \left(\frac{\overline{\rho} Y_{A_k} \Delta z}{(\overline{\rho} Y_{A_k} \Delta z)_{\sum}} \right)^{n_k} \times \exp\left(-\frac{E_k}{RT} \right) g(Y_{O_2}) \tag{2.20}$$

where

$$(\overline{\rho} Y_{A_k} \Delta z)_{\sum} = \overline{\rho} Y_{A_k} \Delta z|_{t=0} + \int_0^t \dot{\omega}'''_{fi}(\tau) \Delta z(\tau) d\tau \ . \tag{2.21}$$

In Eq. (2.20), for inert atmosphere $g(Y_{O_2})$ will be equal to one and for our set of simulations $g(Y_{O_2})$ will be equal to $(1 + Y_{O_2})^{n_{O_2,k}-1}$ for an oxidative atmosphere [1, 21]. Lautenberger and Fernandez-Pello [21] provide additional detail about reaction rate evaluation.

Global kinetic descriptions of smoldering combustion, in general, include reactions for

fuel pyrolysis, fuel oxidation, and char oxidation. We used the kinetic model of Huang and Rein [1]. In the fuel pyrolysis reaction the fuel undergoes thermal degradation in absence of oxygen to produce α-char and gas. In the fuel oxidation reaction, fuel in the presence of oxygen undergoes thermochemical conversion to form β-char and gas. Both α-char and β-char undergo further, separate oxidation reaction to form ash and gas. The smoldering reaction model also includes a drying step if moisture content is present. For this study, the chemical kinetic parameters for smoldering combustion for both cellulose and hemicellulose were obtained from Huang and Rein [1]. (All the reactions used in the model and associated parameters are given in the supplementary material.) For cellulose smoldering the value of the stoichiometric coefficients (υ) were obtained from Kashiwagi and Nambu [2]. The stochiometric coefficient of char from hemicellulose was obtained from Moriana et al. [3], while stochiometric coefficients for ash were obtained by using the relation IC $= \upsilon_{\alpha,hp}\upsilon_{a,\alpha-co} = \upsilon_{a,ho}\upsilon_{a,\beta-co}$, where a, hp, ho, and co stands for ash, hemicellulose pyrolysis, hemicellulose oxidation and char oxidation, respectively [33]. The value for the amount of oxygen consumed, $\upsilon_{O_2,k}$ consumed is calculated using the relation $\upsilon_{O_2,k} = \Delta H/(-13.1)$ MJ/kg [14, 34].

2.3 Results

The results were first validated by comparing propagation speed and mean peak temperature obtained from experimental measurements. Then, the effects of density, fuel composition and moisture content on propagation speed and mean peak temperature were examined. We calculated propagation speed by taking the derivative of depth with respect to time at the depth where the peak temperature at a particular time. Then, we determined the mean peak temperature by taking the average of the peak temperatures at those depths.

2.3.1 Validation against experiments

The validation against the experimental results were done by comparing the downward average propagation speed and mean peak temperature. In the experiments, four thermocouples were placed at 0.0, 2.5, 5.0, and 7.5 cm from the top surface. Figure 2.1 shows the mean propagation speed and the mean peak temperature measured from the

experiments and calculated from our simulations for a range of fuel compositions: 100%, 75%, 50%, and 25% cellulose, with the remainder as hemicellulose. (We did not validate for 100% hemicellulose due to a lack of experimental data.) From Figure 2.1 we can see that for 100% cellulose content, the model overestimates the propagation speed, but as the cellulose content drops the predicted velocities fall within the experimental error bars. The reason for this error could be that the cellulose samples used in the experiments are fibrous whereas the particles used to obtain the specific surface area of cellulose, char, and ash were assumed spherical [31, 32]. Note that the pore size and permeability was calculated using Eq. (2.17) and Eq. (2.18), respectively, for all the condensed-phase species. Other reasons could be the presence of moisture and inorganic content in the fuel, which this model does not consider. The predicted mean peak temperatures lay within 5.5% of the experimentally measured values.

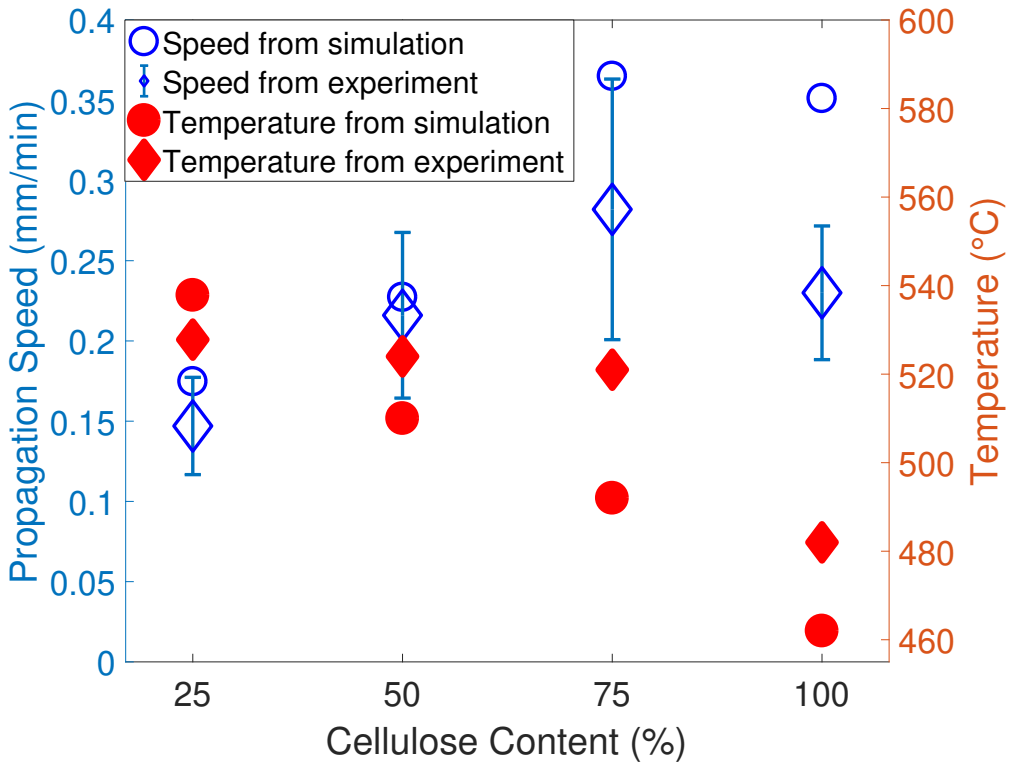

Figure 2.1: Comparison of mean propagation speeds and mean peak temperatures obtained from experiments and simulations.

2.3.2 Effect of fuel composition and density

To examine the effects of fuel composition and density on smoldering combustion, we varied the fuel composition between 100% and 25% cellulose in increments of 25%, where the remaining portion was hemicellulose, and varied the density between 200 and 500 $\mathrm{kg/m^3}$ in increments of 100 $\mathrm{kg/m^3}$. To ignite the sample, we applied a heat flux of 15 $\mathrm{kW/m^2}$ at the top layer for the span of 15 minutes.

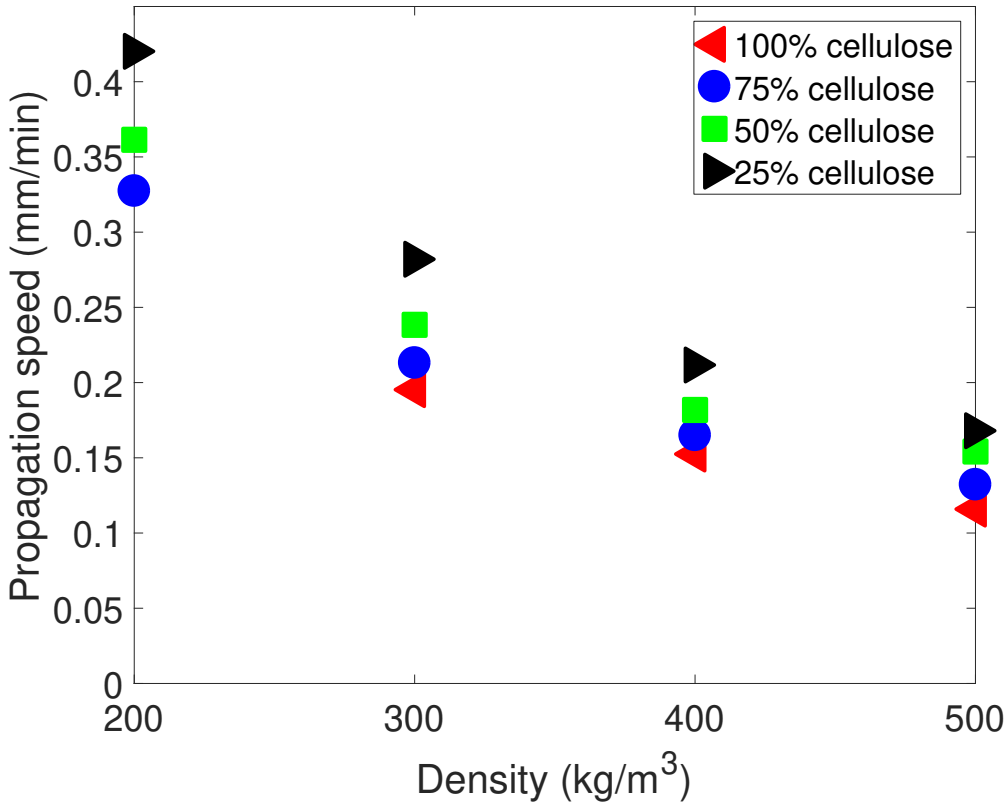

Figure 2.2: Effect of density on mean propagation speed.

Figure 2.2 shows that the propagation speed drops as the density increases for all fuel compositions. The propagation speed drops by around 60% for all the calculated fuel compositions when the density increases from 200 $\mathrm{kg/m^3}$ to 500 $\mathrm{kg/m^3}$. For the aforementioned boundary condition, 100% cellulose at density 200 $\mathrm{kg/m^3}$ did not ignite. This decrease in the propagation speed with increase in density could be due to the fact

that as the density of the fuel sample increases the pore size and permeability of the fuel sample decrease, as expressed in Eqs. (2.17) and (2.18). Due to this relationship, the availability of the oxygen drops as the density increases. Since the smoldering spread rate depends on the oxygen supply [10], less availability of oxygen leads to a reduction in propagation speed. Figure 2.3 shows the mass fraction of oxygen with respect to time at depth 5 cm from the top surface for 100% cellulose. At any point after ignition, more oxygen is available for the fuels with lower density.

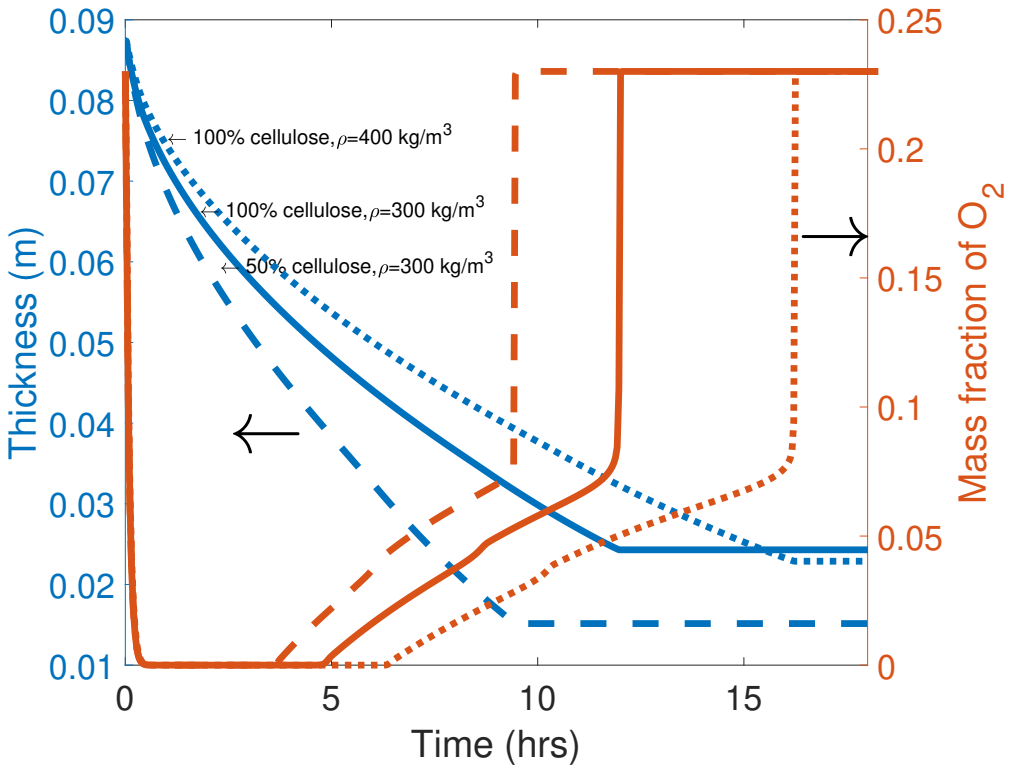

Figure 2.3: Mass fraction of oxygen at depth 5 cm from the top and thickness over time for fuels with 100% cellulose of density 300 kg/m^3 and 400 kg/m^3 and 50% cellulose of density 300 kg/m^3.

Figure 2.2 shows that, for any density between 200 and 500 kg/m^3, fuels with higher cellulose content have slower propagation speeds compared with fuels with higher hemicellulose content. Hemicellulose pyrolyzes at lower temperatures compared with cellulose [35], and as a result there will be more mass loss at an earlier stage from pyrolysis

for samples with more hemicellulose content. This would result in more availability of oxygen for a particular depth since the sample would shrink faster, which can also be seen in Figure 2.3. Figure 2.3 shows that the 50% hemicellulose case has higher mass fraction of oxygen available at earlier times compared with 0% hemicellulose content. More oxygen will promote oxidation and lead to faster propagation.

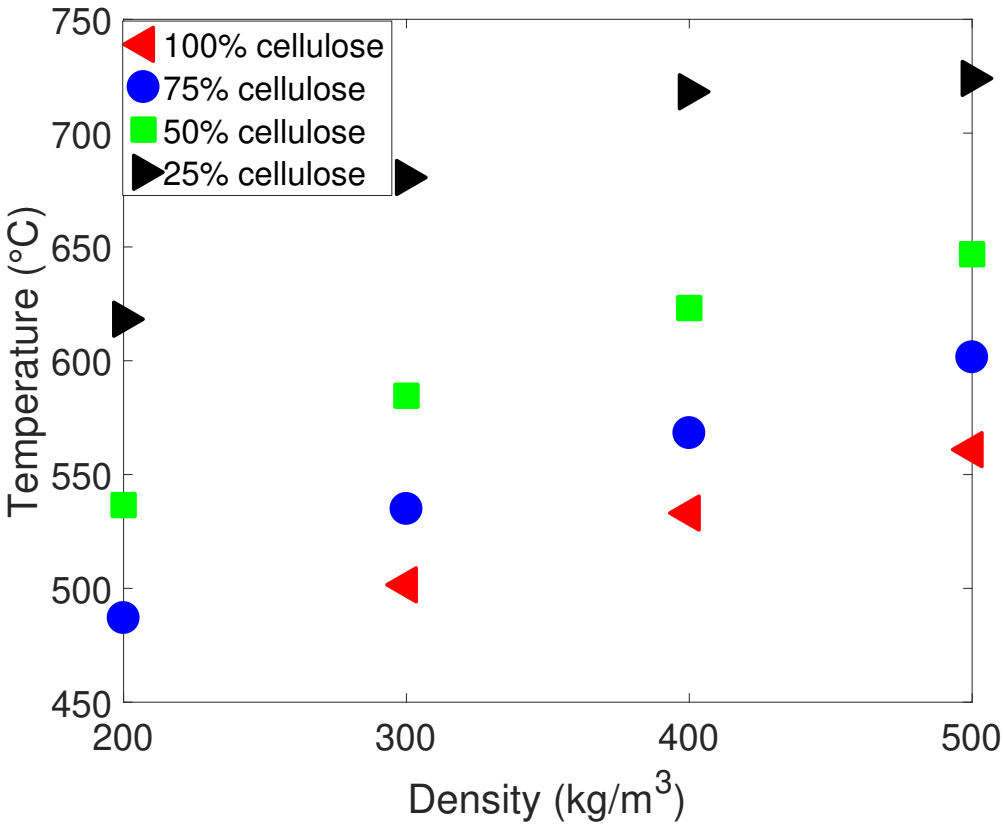

Figure 2.4: Effect of density on mean peak temperature.

Figure 2.4 shows the effects of density and fuel composition on mean peak temperature. The mean peak temperature increases with increasing density as well as hemicellulose content. When hemicellulose content and density is increased, the amount of ash produced also increases because in general hemicellulose has more natural inorganic content than cellulose. Natural inorganic content is directly proportional to the amount of ash produced [33]; further, increasing density makes more fuel available, which results in

formation of more ash. Figure 2.3 shows that the final thickness—which is the area occupied by ash per unit length—is less for fuels with higher density and hemicellulose content, indicating that the densities of ash produced for these fuels are higher. This higher-density ash, which is formed in the top layer, would insulate the sample and retain the heat produced from oxidation. This would result in higher smoldering temperatures, as seen in Figure 2.4.

2.3.3 Effect of moisture content

We considered the effects of moisture content by adding a drying step to the reaction scheme. The reaction parameters for the drying step were obtained from Huang and Rein [1]. Adding water to the sample leads to an expansion in the fuel, which in turn decreases the density of the fuel after the water evaporates. Here, we adopted the co-relation that takes into account this expansion from that used by Huang and Rein [13] for peat.

Figure 2.5 shows the effect of moisture content on propagation speed. The propagation speed increases by 4% as moisture content is increased from 0 to 30%. One of the reasons for this increase is that when water is mixed with the fuel, the fuel will expand, which would eventually lead to reduction in density of the fuel once the water evaporates [13]. In addition, thermal conductivity of the wet fuel increases with moisture content due to the added water [13]. Huang and Rein also observed increases in downward propagation speed of peat with increasing moisture content both experimentally and computationally [13]. After 30% moisture content, the propagation speed did not significantly change further; the propagation speed drops by around 1.5% when the moisture content was increased from 30% to 70%. Figure 2.5 also shows how the propagation speed of 100% cellulose changes due to reduced density due to moisture content, but without the other effects of moisture. The difference between these two velocities indicates how the other effects of moisture content counter the effect of expansion. As we increase the moisture content, both the effects of expansion and moisture content on smoldering grow. However, the increasing difference between the trends shows that the other effects of adding water—such as making the drying step more endothermic, in turn leading to a drop in the overall temperature as Figure 2.5 shows—overcome the expansion effect at higher moisture contents to reduce the propagation speed.

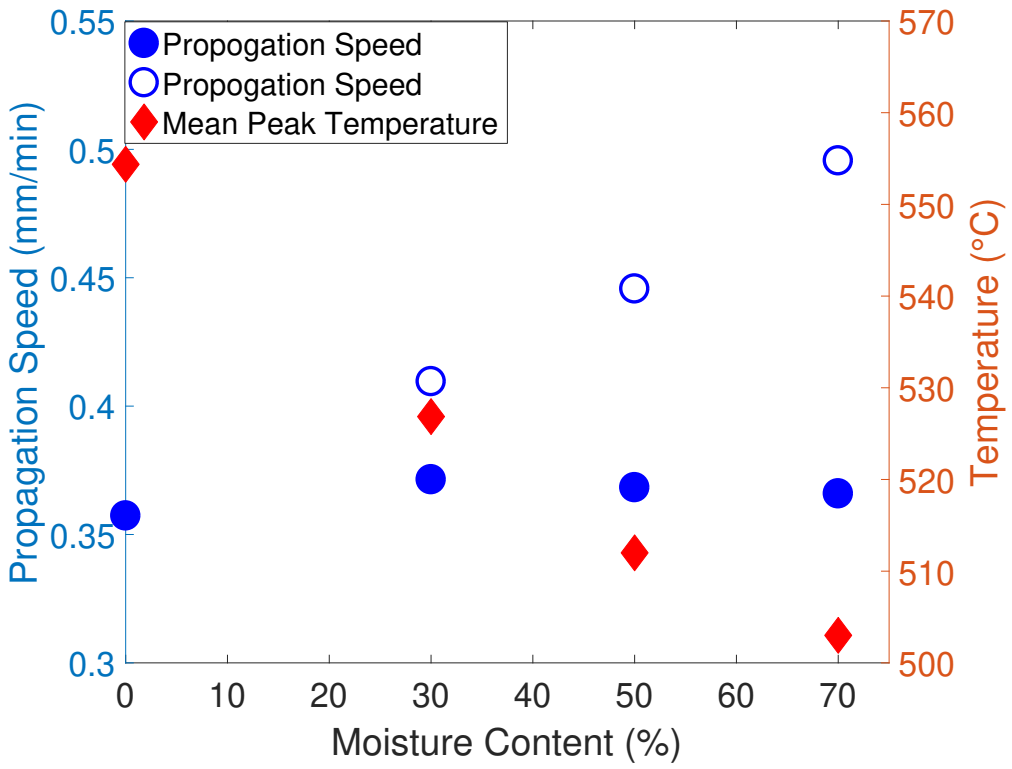

Figure 2.5: Effect of moisture content on mean peak temperature and propagation speed. For propagation speed, filled circles indicate moisture content, while unfilled circles indicate no moisture content but with same amount of natural expansion that would occur if moisture content was added.

(For simulations with high moisture content, i.e., when moisture content is greater than the fiber-saturation point, moisture would be present as capillary water, which is not well approximated with chemical reactions.) Temperature, on the other hand, continuously decreases as moisture content is increased from 0 to 70%. This is because as moisture content increases, more heat is needed to evaporate the water, which reduces the overall temperature.

2.4 Conclusion

In this article, we studied the downward smoldering propagation of cellulose and hemicellulose mixture. First, we validated the model by comparing the values of propagation speed and mean peak temperature against experimentally obtained values for fuel compositions of 100, 75, 50, and 25% of cellulose with remaining portion being hemicellulose. The predicted values of propagation for 75, 50, and 25% cellulose agree with the experimental results within the measurement uncertainty. We suggest that the model overpredicts the values of propagation speed for 100% cellulose due to the calculation that assumed solid particle shapes as spherical, while in reality the particles are fibrous in shape.

Next, we examined the effects of changing density, fuel composition, and moisture content on smoldering propagation speed and mean peak temperature. Propagation speed of smoldering combustion decreases with increases in density and cellulose content. The possible reason for this is lack of availability of oxygen. In the case of density, as the density increases the permeability and pore size drop, which limits the available oxygen. As hemicellulose content increases, more oxygen becomes available due the additional mass that pyrolyzes at a given time, since hemicellulose undergoes pyrolysis at lower temperatures than cellulose. The mean peak temperature increases with density and hemicellulose content, possibly due to more and denser formation of ash on the surface, which acts as an insulator. In the case of moisture content on smoldering combustion for 100% cellulose, the propagation speed increases by about 4% as moisture content increases from 0 to 30%. This is caused by expansion of the fuel when water is added, which reduces the density of fuel when the water evaporates. After this point, the propagation speed only drops by about 1.4% as moisture content increases from 30% to 70%, indicating a lack of sensitivity to moisture content at values above 30%.

Supplementary material

The appendix contains a description of the experimental setup used to provide validation data in this chapter (App. A), the values of kinetic parameters used in the model (App. B), and a grid convergence study (App. D).

Smoldering combustion in cellulose and hemicellulose mixtures: Examining the roles of density, fuel composition, oxygen concentration, and moisture content

Tejas Chandrashekhar Mulky and Kyle E. Niemeyer

In preparation.

Chapter 3: Smoldering combustion in cellulose and hemicellulose mixtures: Examining the roles of density, fuel composition, oxygen concentration, and moisture content

Abstract

Smoldering combustion plays a major role in wildfires in forests, grasslands, and peatlands due to its common occurrence in porous fuels like peat and duff. As a consequence, understanding smoldering behavior in these types of fuel is crucial. Such fuels are generally composed of cellulose, hemicellulose, and lignin. Here I present an updated computational model for simulating smoldering combustion in cellulose and hemicellulose mixtures. I used this model to examine changes in smoldering propagation speed and peak temperatures on varying fuel composition and density. For a given fuel composition, increases in density reduce the propagation speed and mean peak temperature; for a given density, increases in hemicellulose content increase both propagation speed and mean peak temperature. Temperature drops with increases in density due to the higher solid thermal conductivity of condensed-phase species, and temperature increases with hemicellulose content due to formation of lower-thermal-conductivity ash at the surface. Propagation speed increases with hemicellulose content due to quicker pyrolysis of hemicellulose resulting in faster access to oxygen, while propagation speed increases with reduction in density due to less mass to be converted into char and ash, again resulting in faster access to oxygen. I then used the model to examine the role of natural fuel expansion with the addition of water. Without expansion, addition of moisture content reduces the propagation speed primarily due to increasing density of the wet fuel. However, with fuel expansion similar to that observed in peat, the propagation speed increases due to the overall drop in fuel density. Finally, I examined the influence of fuel composition on critical moisture content of ignition and extinction, and found that mixtures dominated by hemicellulose (e.g., 75% or more) have 10% higher critical moisture content due to the increase in mean peak temperature.

3.1 Introduction

Wildland fires lead to human, environmental and ecological hazards. In recent time due to climate change, it has been predicted that there will be an increase in the occurrence of droughts which would eventually lead to an increase in the frequency of wildland fires [36, 37]. Combustion in wildland fires, in general, is dominated by either flaming or smoldering combustion. Both types of combustion have different characteristics and can be hazardous in their own way. There has been a lot of work done over the years to understand flaming combustion compared to smoldering combustion [10]. However, in recent years smoldering combustion has been recognized as one of the major fire hazards which resulted in an increasing interest to understand this phenomenon [10].

Smoldering combustion is a persistent type of combustion. This characteristic of smoldering combustion leads to deeper penetration in the soil compared to flaming combustion which generally causes shallower burns [38, 39]. This behavior of smoldering combustion eventually leads to a greater destruction of the ecosystem. Smoldering also emits a large number of pollutants since it operates at lower temperatures compared to flaming combustion. Smoldering combustion occurs most commonly in porous fuels like peat, woody fuels, and forest duff [37]. Such fuels are available in abundance in forests which makes understanding smoldering combustion in these types of fuel important. The above-mentioned fuels are generally made up of cellulose, hemicellulose, and lignin. Cellulose, hemicellulose, and lignin pyrolyze at different temperatures. Yang et al. [40] found that among the three, hemicellulose pyrolyzes the earliest, at a temperature range of 220–315 °C after which cellulose undergoes pyrolysis at the temperature range of 315–400 °C and lignin undergoes pyrolysis at the temperature range of 150–900 °C. Also, the amount of char produced by these individual constituents can be different [1, 2, 41]. Smoldering combustion, in general, is represented by a group of global pyrolysis and oxidation reactions which include fuel pyrolysis and char oxidation reactions [9]. This is the reason that there could be significant difference in smoldering characteristics on the change in the fuel composition. Hence a detailed study is required that looks into the effects of varying fuel composition on smoldering characteristics.

Along with fuel composition, the other parameters that could affect smoldering propagation are density and moisture content. Huang and Rein [13] found that when the density of peat was increased by 40% the downward propagation speed reduced by ap-

proximately 40%. However, there has been no computational work that looked into how changes in density affect smoldering speed and temperatures in fuel mixtures of cellulose and hemicellulose. There has been some work done that looked into the effects of moisture content on smoldering combustion: Huang and Rein studied how moisture content affects propagation speed of peat, and observed an increase in propagation speed with moisture content for downward propagation due to expansion in peat [13]. Recently, Smucker et al. [42] experimentally observed that smoldering propagation speed in mixtures of cellulose and hemicellulose decreases with density, and attributed this to oxygen availability. In addition, they found that propagation speed increases with additional hemicellulose content in fuel, attributed to the higher temperatures and faster pyrolysis with addition of hemicellulose.

Critical moisture content is the highest moisture content above which smoldering combustion cannot self-sustain. Garlough and Keyes [43] experimentally studied ponderosa pine duff and found that fuel consumption decreases after reaching critical moisture content of 57 and 102% on the upper and lower duff, respectively. Huang and Rein [44] found that peat's critical moisture contents of ignition and extinction are around 117% and 250%, respectively, depending upon the thickness of wet layer, dry layer, and boundary conditions. However, no studies have looked into the influence of the fuel composition on these threshold values.

In my previous work, I found that propagation speed increases as density drops or hemicellulose content increases for mixtures of cellulose and hemicellulose [45]. Based on prior theories in the literature, I hypothesized that oxygen availability causes the sensitivity to density, and earlier pyrolysis of hemicellulose as the reason for the faster propagation with its addition. However, I did not perform an in-depth analysis to examine the proposed hypotheses. In addition, for validating the model with experimental results, I relied on a fixed temperature boundary condition, which overconstrained the model. Furthermore, my treatment of bulk density in that work may not represent actual experimental conditions: the bulk density of hemicellulose was fixed, and I changed the bulk density of cellulose to match the mixture bulk density; in reality, Also, the model used in that work could not predict ignition for at bulk densities of less than $200\,\mathrm{kg/m^3}$ for 100% cellulose, which disagrees with experimental observations [42].

Building on my prior work, this article proposes an updated one-dimensional, transient computational model to simulate smoldering combustion in cellulose and hemicellulose

mixtures. First, I validate the model against a different experimental configuration that more closely matches the simulation, and use a heat-flux boundary condition. Following this model validation, I examine the effects of varying density and fuel composition on smoldering propagation speed and peak temperature, and perform and in-depth analysis to explain the observed trends. Next, I investigate the effects of varying moisture content on smoldering propagation speed and temperature, including and excluding the contribution of fuel expansion with the addition of water. I then identify how varying fuel composition affects the critical moisture content of ignition and extinction. Finally, I summarize my conclusions and identify paths for future study.

3.2 Computational model

In this paper, I focus on downward propagation of smoldering using a one-dimensional transient model following approaches of past studies [45]. This model was developed using Gpyro [22]. Simulations were run with a cell size (Δz) of 1×10^{-4} m and an initial time step of 0.05 s. The selection of cell size was based on my previous work, where I showed that further improving resolution has little impact on global quantities of interest [45].

3.2.1 Governing equations

To model smoldering combustion condensed phase mass conservation (3.1), condensed phase species conservation (3.2), gas phase mass conservation (3.3), gas phase species conservation (3.4), condensed phase energy conservation (3.5), gas phase momentum conservation (3.6), gas phase energy conservation (3.7) and ideal gas law (3.8) to close the set of equation needs to be solved. These transient governing equations were solved using Gpyro software. More details about Gpyro is provided in Lautenberger and Fernandez-Pello [21].

$$\frac{\partial \overline{\rho}}{\partial t} = -\dot{\omega}'''_{fg} \,, \tag{3.1}$$

$$\frac{\partial (\overline{\rho} Y_i)}{\partial t} = \dot{\omega}'''_{fi} - \dot{\omega}'''_{di} \,, \tag{3.2}$$

$$\frac{\partial (\rho_g \overline{\psi})}{\partial t} + \frac{\partial \dot{m}''}{\partial z} = \dot{\omega}'''_{fg} \,, \tag{3.3}$$

$$\frac{\partial(\rho_g\overline{\psi}Y_j)}{\partial t}+\frac{\partial(\dot{m}''Y_j)}{\partial z}=-\frac{\partial}{\partial z}(\overline{\psi}\rho_g D\frac{\partial Y_j}{\partial z})+\dot{\omega}'''_{fj}-\dot{\omega}'''_{dj}\ , \tag{3.4}$$

$$\frac{\partial(\overline{\rho}\overline{h})}{\partial t}=\frac{\partial}{\partial z}(\overline{k}\frac{\partial T}{\partial z})-\dot{Q}'''_{s-g}+\sum_{k=1}^{K}\dot{Q}'''_{s,k}-\frac{\partial \dot{q}''_r}{\partial z}$$
$$+\sum_{i=1}^{M}((\dot{\omega}'''_{fi}-\dot{\omega}'''_{di})h_i)\ , \tag{3.5}$$

$$\dot{m}''=-\frac{\overline{K}}{v}\frac{\partial P}{\partial z}\ ,\ \text{and} \tag{3.6}$$

$$\frac{\partial(\overline{\psi}\rho_g\overline{h_g})}{\partial t}+\frac{\partial(\dot{m}''_z\overline{h_g})}{\partial z}=\frac{\partial}{\partial z}(\overline{\psi}\rho_g D\frac{\partial\overline{h_g}}{\partial z})+h_{cv}(T-T_g)$$
$$+\sum_{j=1}^{N}(\dot{\omega}'''_{s,fj}-\dot{\omega}'''_{s,dj})h^*_{g,j}+\dot{Q}'''_{s-g}\ , \tag{3.7}$$

$$P\overline{M}=\rho_g RT_g\ , \tag{3.8}$$

where ρ is the density, M is the number of condensed-phase species; X is the volume fraction; $\dot{\omega}'''$ is the reaction rate; T is the temperature; Y_j is the jth species mass fraction; ψ is the porosity; K is the permeability/number of reactions; h_{cv} is the volumetric heat transfer coefficient; $\overline{M}$ is the mean molecular mass obtained from local volume fractions of all gaseous species; $\dot{q}''_r$ is the radiative heat-flux; $\dot{Q}'''$ is the volumetric rate of heat release/absorption; R is the universal gas constant; D is the diffusion coefficient; h is the enthalpy; P is the pressure; subscripts f, d, i, j, k, s, and g are formation, destruction, condensed-phase species index, gas-phase species index, reaction index, solid, and gas;* is used to indicate that gas phase species enthalpy is calculated at condensed phase temperature. The overbar over ρ, ψ, K, k indicates an averaged value weighted by condensed-phase volume fraction, while the overbar over h indicates averaged value weighted by condensed-phase mass fraction.

3.2.2 Boundary conditions

The top surface ($z=0$) of the domain was modeled to be open to atmosphere while the bottom surface ($z=L$) was modelled to be insulated to match the experimental setup. The pressure (P) at the top surface was set to 1 atm and the ambient temperature was set

to 300 K. On the top surface a convective heat transfer coefficient ($h_{c,0}$) was set 10 W/m^{2}K using the an empirical correlation of $h_{c,z=0} = 1.52 \times (T)^{1/3}$ where $T = 300$ K [14]. On the top surface a mass transfer coefficient ($h_{m,0}$) was set equal to 0.02 kg/m^2 sec based on previous work [14]. To ignite the sample a heat flux ($\dot{q}''_e$) of 25 kW/m^2 was provided for 20 min so that a self-sustained smoldering combustion is established after which the heat flux was removed and a convective–radiative balance was established at the top surface which is shown in Eqs. (3.9) and (3.10), respectively. This boundary condition was applied for all simulations except for those where I looked at effects of varying moisture content on propagation speed (Sec. 3.3.3) where I provided a constant heat flux throughout the experiment to establish ignition at higher moisture contents. The equations used for boundary condition on the top surface are:

$$-\overline{k}\frac{\partial T}{\partial z}\bigg|_{z=0} = -h_{c0}(T_{z=0} - T_\infty) + \overline{\epsilon}\dot{q}''_e - \overline{\epsilon}\sigma(T^4_{z=0} - T^4_\infty)] \,, \tag{3.9}$$

$$-\overline{k}\frac{\partial T}{\partial z}\bigg|_{z=0} = -h_{c0}(T_{z=0} - T_\infty) - \overline{\epsilon}\sigma(T^4_{z=0} - T^4_\infty) \,, \tag{3.10}$$

$$-\left(\overline{\psi}\rho_g D\frac{\partial Y_j}{\partial z}\right)\bigg|_{z=0} = h_{m0}\left(Y_{j\infty} - Y_j|_{z=0}\right) \text{ , and} \tag{3.11}$$

$$P|_{z=0} = P_\infty \,. \tag{3.12}$$

For the bottom surface a heat transfer coefficient ($h_{c,L}$) was set equal to 3 W/m^{2}K. This was done to ensure that the losses from the insulation is taken into account for. While the mass flux ($\dot{m}''$) was set to zero in the bottom surface. The equations used for boundary condition on the bottom surface are:

$$-\overline{k}\frac{\partial T}{\partial z}\bigg|_{z=L} = -h_{cL}(T|_{z=L} - T_\infty) \,, \tag{3.13}$$

$$-(\overline{\psi}\rho_g D\frac{\partial Y_j}{\partial z})\bigg|_{z=L} = h_{mL}(Y_{j\infty} - Y_j|_{z=L}) \text{ , and} \tag{3.14}$$

$$\dot{m}''|_{z=L} = 0 \,. \tag{3.15}$$

3.2.3 Chemical kinetics

A heterogeneous reaction is represented in Gpyro as follows [21]:

$$\mathrm{A}_k + \sum_{j=1}^{N} v'_{j,k}\,\mathrm{gas\,j} \longrightarrow v_{B,k}\,\mathrm{B}_k + \sum_{j=1}^{N} v''_{j,k}\,\mathrm{gas\,j} \tag{3.16}$$

The reaction rates are expressed using Arrhenius law as follows [21]:

$$\dot{\omega}'''_{dA_k} = Z_k \frac{(\overline{\rho} Y_{A_k} \Delta z)_{\sum}}{\Delta z} \left(\frac{\overline{\rho} Y_{A_k} \Delta z}{(\overline{\rho} Y_{A_k} \Delta z)_{\sum}} \right)^{n_k} \times \exp\left(-\frac{E_k}{RT}\right) g(Y_{O_2}) \;, \tag{3.17}$$

where

$$(\overline{\rho} Y_{A_k} \Delta z)_{\sum} = \overline{\rho} Y_{A_k} \Delta z|_{t=0} + \int_0^t \dot{\omega}'''_{fi}(\tau) \Delta z(\tau) d\tau \;. \tag{3.18}$$

Where Z is the pre-exponential factor, E is the activation energy, n is the order of reaction, subscript dA stands for destruction of species A and k stands for reaction number. In Eq. (3.17), for inert atmosphere $g(Y_{O_2}) = 1$ and oxygen is available $g(Y_{O_2}) = (1 + Y_{O_2})^{n_{O_2,k}} - 1$ [21].

Smoldering, in general, is represented by a group of global pyrolysis and oxidation reactions [9, 11]. In this work, I use the model developed by Huang and Rein to represent smoldering [1, 33]. In this model fuel first undergoes drying, then the dried fuel undergoes thermal decomposition to form char by two paths: fuel pyrolysis and fuel oxidation. The char obtained from fuel pyrolysis is called α-char while the char obtained from fuel oxidation is called β-char. Then this α and β-char undergoes oxidation reactions to form ash. The drying and fuel pyrolysis reactions are endothermic reactions while the fuel and char oxidation reactions are exothermic. If the fuel is 100% cellulose then I use five global reactions and if the fuel is a mixture of cellulose and hemicellulose then I use 10 global reactions:

$$\mathrm{Cellulose} \cdot v_{w,dr}\mathrm{H_2O} \longrightarrow \mathrm{Cellulose} + v_{w,dr}\mathrm{H_2O\,(g)} \tag{3.19}$$

$$\mathrm{Cellulose} \longrightarrow v_{\alpha,cp}\alpha\mathrm{-Char}_c + v_{g,cp}\mathrm{Gas} \tag{3.20}$$

$$\text{Cellulose} + v_{O_2,co}\text{O}_2 \longrightarrow v_{\beta,co}\beta\text{−Char}_c + v_{g,co}\text{Gas} \tag{3.21}$$

$$\alpha\text{-Char}_c + v_{O_2,c\alpha o}\,\text{O}_2 \longrightarrow v_{a,c\alpha o}\text{Ash}_c + v_{g,c\alpha o}\text{Gas} \tag{3.22}$$

$$\beta\text{-Char}_c + v_{O_2,c\beta o}\text{O}_2 \longrightarrow v_{a,c\beta o}\text{Ash}_c + v_{g,c\beta o}\text{Gas} \tag{3.23}$$

$$\text{Hemicellulose}\cdot v_{w,dr}\text{H}_2\text{O} \longrightarrow \text{Hemicellulose} + v_{w,dr}\text{H}_2\text{O}\,(\text{g}) \tag{3.24}$$

$$\text{Hemicellulose} \longrightarrow v_{\alpha,hp}\alpha\text{−Char}_h + v_{g,hp}\text{Gas} \tag{3.25}$$

$$\text{Hemicellulose} + v_{O_2,ho}\text{O}_2 \longrightarrow v_{\beta,ho}\beta\text{−Char}_h + v_{g,ho}\text{Gas} \tag{3.26}$$

$$\alpha\text{-Char}_h + v_{O_2,h\alpha o}\text{O}_2 \longrightarrow v_{a,h\alpha o}\text{Ash}_h + v_{g,h\alpha o}\text{Gas} \tag{3.27}$$

$$\beta\text{-Char}_h + v_{O_2,h\beta o}\text{O}_2 \longrightarrow v_{a,h\beta o}\text{Ash}_h + v_{g,h\beta o}\text{Gas} \tag{3.28}$$

where v is the stoichiometric coefficient; α and β indicate char produced from fuel pyrolysis and fuel oxidation reactions, respectively; and subscripts w, g, O_2, a, c, h, dr, o, p, αo, βo are water, gas, oxygen, ash, cellulose, hemicellulose, drying, oxidation, pyrolysis, α-char oxidation, and β-char oxidation, respectively. The reaction and chemical kinetic parameters like pre-exponential factor, activation energy, order of reaction, and heat of reaction to represent smoldering in cellulose and hemicellulose were obtained from the peat model of Huang and Rein [1]. Stochiometric coefficients for cellulose were obtained from Kashiwagi and Nambu and for hemicellulose were obtained from Huang and Rein [1, 2]. The values of kinetic parameters used are provided in the supplementary material. The consumption of oxygen was accounted using the relation: $v_{\text{O}_2,k} = \Delta H/(-13.1)$ MJ/kg [14, 34].

3.2.4 Physical properties

The bulk densities of the cellulose and hemicellulose were experimentally measured. The measured natural bulk densities of the cellulose and hemicellulose are 175 kg/m^3 and 695.71 kg/m^3, respectively [20]. Other physical properties which include solid density, thermal conductivity, and heat capacity is reported in Table 3.1. The bulk densities of char were obtained using the correlation $\rho_{\text{char}} \approx \upsilon_{\text{char}} \times \rho_{\text{fuel}}$ [13] and the bulk density of ash were obtained using the correlation $\rho_{\text{ash}} \approx \text{AC}/100 \times 10 \times \rho_{\text{fuel}}$, where AC stands for ash content [23]. The AC for cellulose and hemicellulose is taken as 0.3% and 1.2%, respectively [1, 3, 46]. Based on previous studies I assume physical properties of the fuel to be independent of temperature [14].

Table 3.1: Thermophysical properties of condensed phase species

Species	Solid density (kg/m^3)	Thermal conductivity ($W/(m\,K)$)	Heat capacity ($J/(kg\,K)$)	Source
Water	1000	0.6	4186	[14]
Cellulose	1500	0.356	1674	[24]
Hemicellulose	1365	0.34	1200	[25–27]
Char	1300	0.26	1260	[1, 28]
Ash	2500	1.2	880	[1, 28]

The effective thermal conductivity of the porous fuel is calculated using the equations $k_i = k_{s,i} + \gamma_i \sigma T^3$, which takes into account contributions from both solid and radiative components where the radiative component of the thermal conductivity takes into account the radiation across the pores [21].

The physical properties of the fuel like pore size, parameter controlling radiation across pores, and permeability were calculated at natural densities using the correlations [1, 14, 29, 30]:

$$d_{po,i} \approx d_{p,i} = \frac{1}{S_i \times \rho} \tag{3.29}$$

$$K \approx 10^{-3} \times d_{p,i}^2 \tag{3.30}$$

$$\gamma_i \approx 3 \times d_{po,i}\ , \tag{3.31}$$

Where ρ is the density of the fuel, S is the particle surface area, d_p is the particle size, K is the permeability, and d_{po} is the pore size. The values of particle surface area of cellulose, ash obtained from cellulose, hemicellulose, and ash obtained from hemicellulose are 0.0388, 0.1533, 0.0678, and $0.2712\,m^2/g$, respectively [1, 31, 32, 47]. These correlations are used at natural densities of the fuel based on the assumption that particle size and pore size are similar [1, 14]. When the fuel density is changed by compression the particle size remains the same but pore size reduces due to the reduction of the pore volume. Hence, on compression, the change in pore size and parameter controlling radiation across the pores are accounted by scaling it with change in porosity (ψ) since porosity is directly proportional to the volume occupied by pores. Similarly, change in solid thermal

conductivity is scaled with $(1-\psi)$ since $(1-\psi)$ it is directly proportional to the volume occupied by the solid [14]. Change in permeability due to compression is taken into account using Kozeny-Carman equation which is $K \propto e^3/(1+e)$ where e is the void ratio.

If not mentioned otherwise all the simulation were run with 10% moisture content in order to take into account the moisture content already present in the fuel and moisture absorbed by the fuel from the atmosphere [1, 13]. Addition of moisture content, the change in the density of the wet fuel is calculated using the following equation $\rho_{wetfuel} = \rho_{dryfuel} \times (1+MC)$ where MC is the moisture content [14]. If the fuel is expanding on addition of water then I use the correlation developed for peat by Huang and Rein [13] with bulk density modified for the fuel here. Since the change in the porosity on modification of density is not more than 5% this modification is justified. The modified correlation is: $\rho_{dryfuel} = (200+40MC)/(1+MC)$. The change in the thermal conductivity (k) and heat capacity (c) of the wet-fuel are obtained by averaging either using volume fraction (X_i) or mass fraction (Y_i) as shown: $k_{wetfuel} = X_{H_2O}k_{H_2O} + X_{dryfuel}k_{dryfuel}$ and $c_{wetfuel} = Y_{H_2O}c_{H_2O} + Y_{dryfuel}c_{dryfuel}$ [14, 21].

3.2.5 Calculation of global quantities

The two parameters of interest in this study are mean propagation speed and mean peak temperature. Propagation speed is calculated by taking derivatives of depths with respect to time when the peak temperature occurs at the respective depths. To determine the appropriate value of the depth interval for calculating mean propagation speed between 1 cm and 6 cm, I systematically reduced the depth interval and examined its effect on mean propagation speed. If I reduce the value of depth interval by a factor of two smaller than 1 cm (i.e., to 0.5 cm), the mean propagation does not change more than 0.3%. Hence a 1 cm depth interval was used for all simulations. Appendix E contains a figure showing the effects of reducing depth interval on propagation speed. Mean peak temperature was calculated similarly by averaging the peak temperatures at every 1 cm depth interval.

3.3 Results and discussion

I first validated the model against experimental results by comparing it with measured values of mean peak temperature and mean propagation speed. Then I performed a sensitivity analysis of these two parameters by varying density and fuel composition. I then examined the effect of increasing the moisture content on mean peak temperature and mean propagation speed on 100% cellulose. Finally, I studied how the critical moisture contents of ignition and extinction change with fuel composition.

3.3.1 Validation

The computational model is validated against experimental results by comparing it with two parameters: mean peak temperature and mean propagation speed. The experiments were conducted in a 1D reactor box with the dimensions of $10 \times 10 \times 13\,\text{cm}$. The thermocouples in the reactor box were placed at 1 cm intervals. The top surface of the reactor box was open to the atmosphere and all the other sides were insulated using a calcium silicate insulation board. The fuel sample was ignited using a 20 W cartridge heater. More details about the experimental set-up can be obtained from Smucker et.al [42]. A preliminary energy balance across the cartridge heater showed that 20 W cartridge heater approximately equals to $25\,\text{kW/m}^2$ heat flux. Hence for simulations a heat flux of $25\,\text{kW/m}^2$ is applied for 20 min and then removed in order to establish a self-sustained smoldering. Even when the heat flux was increased by a factor of 2 the propagation speed changed by less than 1.8%. Hence this gave us the confidence to use heat flux as the boundary condition to ignite the fuel sample.

Four fuel samples with different fuel compositions which include 100% cellulose, 75% cellulose 25% hemicellulose, 50% cellulose 50% hemicellulose, 25% cellulose 75% hemicellulose with different respective densities of $170\,\text{kg/m}^3$, $300\,\text{kg/m}^3$, $250\,\text{kg/m}^3$, $400\,\text{kg/m}^3$ were used to validate the model. In Figure 3.1, the model qualitatively captures all the trends both in the propagation velocity and temperature. The maximum percentage error in the predicated propagation speed is observed in fuel with 100% cellulose which is 11.06% while the average percentage error for all the four sample is around 6.36%. Similarly, the maximum percentage error in the mean peak temperature is observed in fuel with 100% cellulose which is around 6.5% while the average percentage error for all

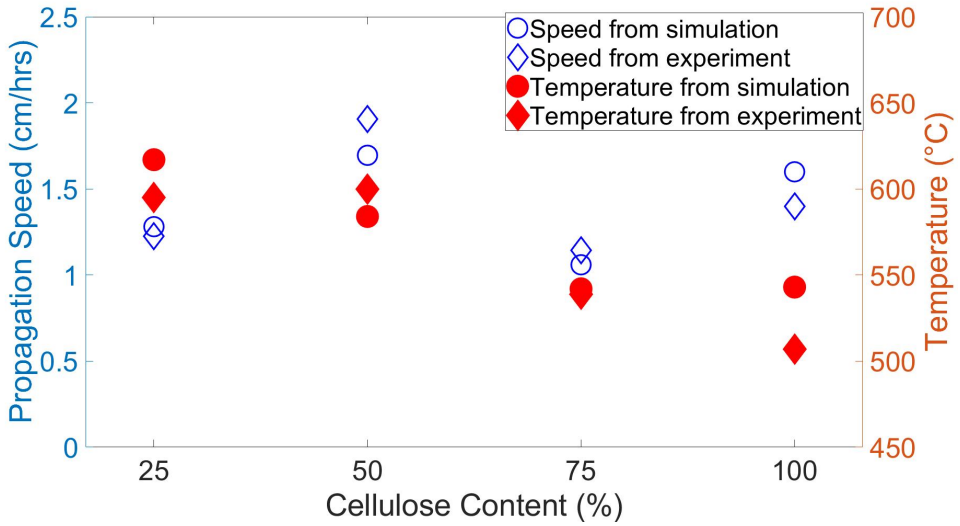

Figure 3.1: Experimentally obtained and predicted propagation speed and mean peak temperature for fuel composition 100% cellulose, 75% cellulose, 50% cellulose, and 25% cellulose at density 170 kg/m^3, 300 kg/m^3, 250 kg/m^3, and 400 kg/m^3

the four sample is around 3.3%. So I conclude that the model successfully predicts the mean peak temperatures and mean propagation speed for the above mentioned mixtures, and I can use it with confidence for the remaining studies.

3.3.2 Sensitivity to fuel composition and density

Next, I study the effect of density and fuel composition on mean peak temperatures. Fuel density was varied between 200-400 kg/m^3 with an increment of 50 kg/m^3 and the fuel composition was varied from 100% cellulose to 25% cellulose with decrements of 25% cellulose where the remaining fuel is hemicellulose. Figure 3.2 shows the effect of fuel density and fuel composition on mean peak temperature. In Fig. 3.2, as the density of the fuel increases there is a drop in mean peak temperatures. In order to explain the reason behind this temperature dependence, parameters that change when density increases were varied individually. From this study it was found that peak temperatures decreases with increase in density because of the increase in the solid thermal conductivity of all the condensed phase species on increase in density. Figure 3.4 shows temperature profile

of 100% cellulose at density 200 kg/m^3, 400 kg/m^3, and 200 kg/m^3 with solid thermal conductivity of 400 kg/m^3. For fuel with density 200 kg/m^3, when only the values of solid thermal conductivity of condensed phase species is changed from 200 kg/m^3 to 400 kg/m^3, the peak temperatures becomes approximately equals to the fuel with density 400 kg/m^3 which proves my claim.

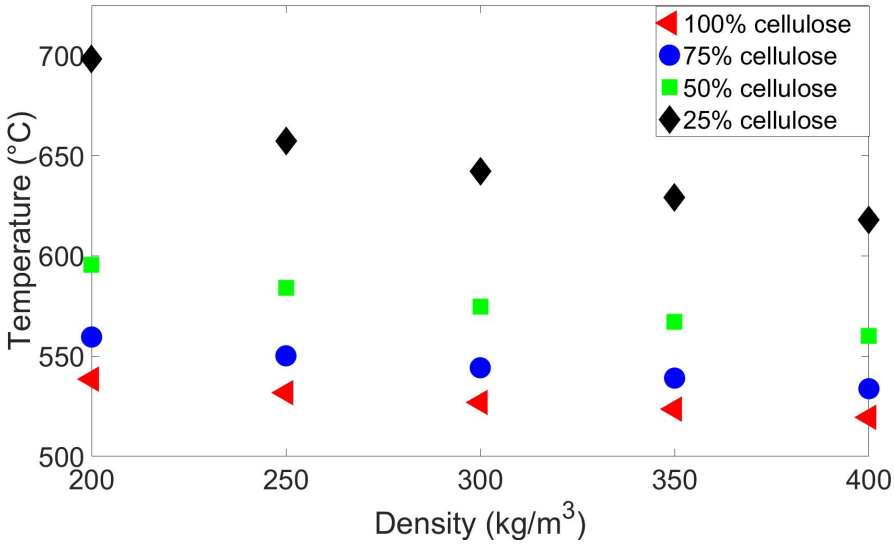

Figure 3.2: Effects of varying density and fuel composition on temperature

In Fig. 3.2, the other trend that is observed is when hemicellulose content in the fuel increases the mean peak temperature of the fuel also increases. In order to explain this Figure 3.3 shows the temperature contour at varying depth and time for 50% cellulose and 50% hemicellulose at fuel density 300 kg/m^3. The peak temperatures in Fig. 3.3 are not attained at the surface of the fuel where oxygen is most available but is attained below the surface. The reason for this is that ash is formed at the topmost layer of the fuel. This makes the thermal conductivity of ash important since it acts as an insulation layer on top. The effective thermal conductivity of ash coming from cellulose is greater at given density compared with ash coming from hemicellulose. This is due to the larger pore size of ash from cellulose compared to ash from hemicellulose which leads to greater losses due to radiation across the pores. I tested this by performing simulations where the effective thermal conductivity of ash from hemicellulose was matched to ash from

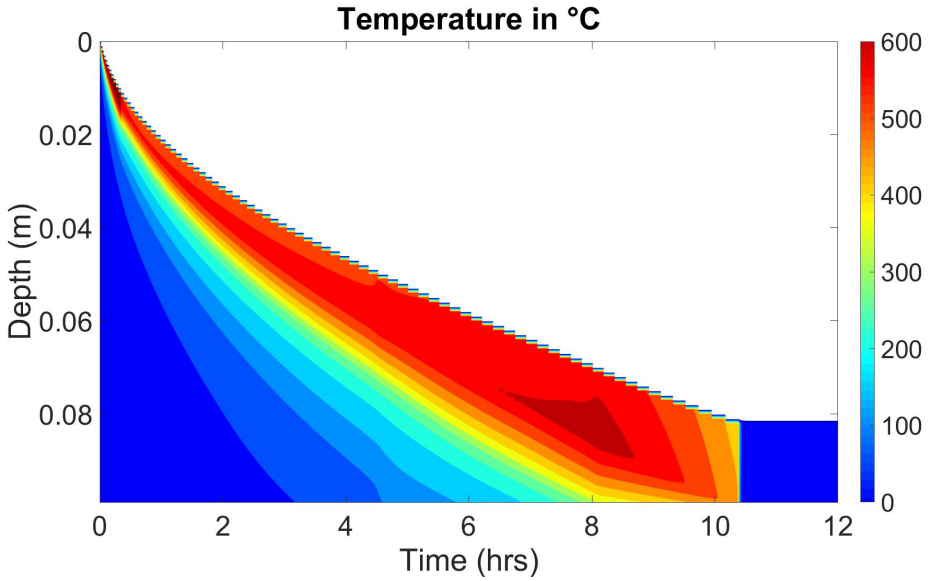

Figure 3.3: Temperature contour varying with depth and time for fuel composition of cellulose 50% and density of 300 kg/m^3

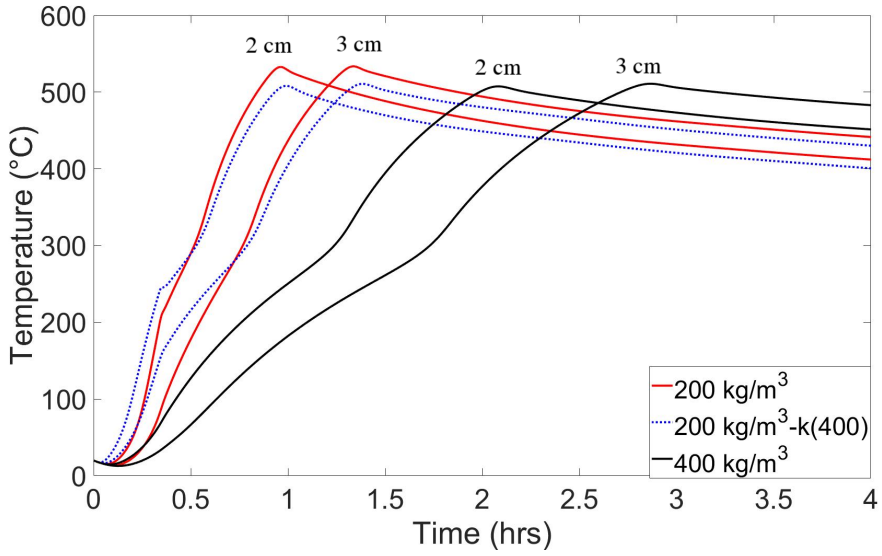

Figure 3.4: Temperature profiles at depth 2 and 3 cm of 100% cellulose with densities 200 kg/m^3, 300 kg/m^3, and 200 kg/m^3 with solid thermal conductivity of 300 kg/m^3

cellulose for fuel with 50% cellulose at density 300 kg/m^3. Temperature profiles for this simulation which is shown in Figure 3.5 along with temperature profiles of 50% cellulose and 100% cellulose at density 300 kg/m^3. Since, the peak temperatures of fuel with 50% cellulose becomes equal to 100% cellulose when the thermal conductivity of ash from cellulose and hemicellulose are made equal to cellulose this justifies my claim. Hence the overall temperature variations observed due to density and fuel composition is mainly due to the variation in the thermal conductivity of the condensed phase species. In both Fig. 3.4 and Fig. 3.5 it should be also noted that even if there is a drop in mean peak temperatures the position of the peak temperature is not shifted significantly, indicating that this change in peak temperatures does not significantly affect propagation speed.

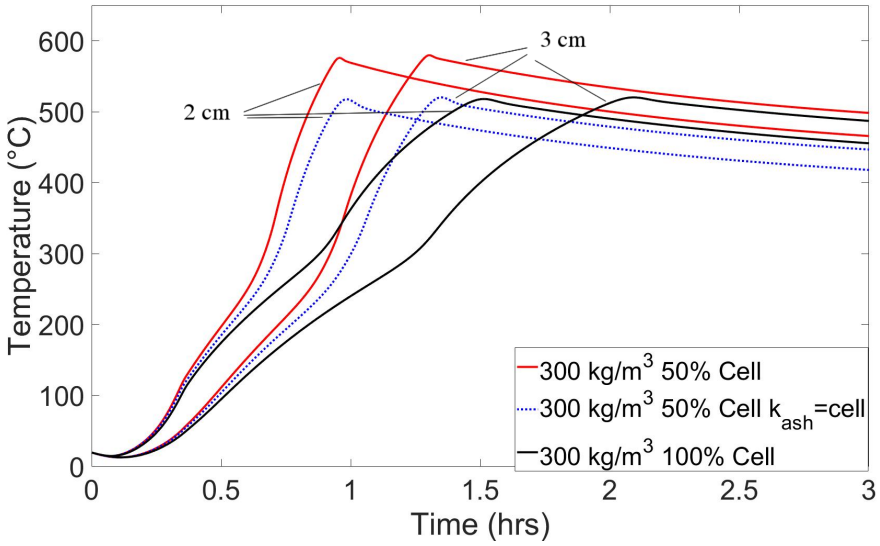

Figure 3.5: Temperature profiles at depth 2 and 3 cm for fuels with density 300 kg/m^3 and fuel composition of 50% cellulose, 100% cellulose, and 50% cellulose with thermal conductivity of ash coming hemicellulose set equal to cellulose.

Now I look into the effects of density and fuel composition on mean propagation speed shown in Figure 3.6. In Fig. 3.6 when hemicellulose is added to the fuel the propagation speed of smoldering combustion increases. To understand this, reaction rates of fuel with hemicellulose at time 4000 s along the depth is shown in Figure 3.7. When hemicellulose is added to the fuel sample, at a given time hemicellulose undergoes pyrolysis at a deeper

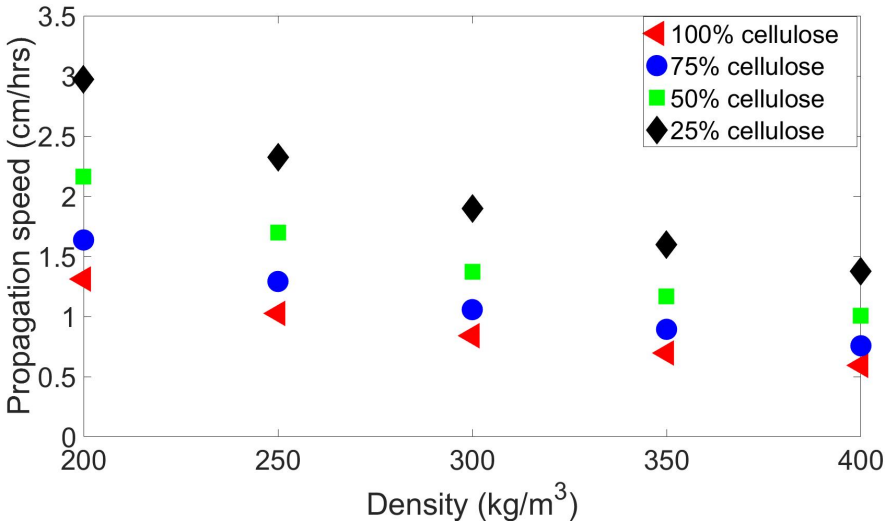

Figure 3.6: Effects of varying density and fuel composition on propagation speed

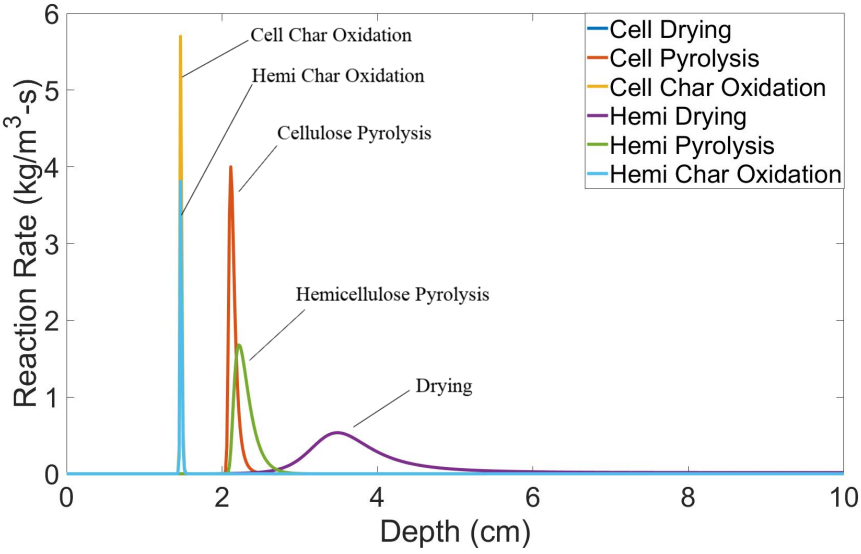

Figure 3.7: Reaction rates for 50% cellulose and 50% hemicellulose at density 300 kg/m^3 along the depth at a time 4000 s

depth before cellulose. This leads to faster shrinkage of the fuel giving quicker access to oxygen ultimately leading into faster propagation speed. Figure 3.6 also shows that when the density of the fuel increases the propagation speed of smoldering combustion decreases for all fuel composition. Figure 3.8 shows the reaction rates and condensed phase species mass fraction at depth 4 cm from the top for fuels with composition of 100% cellulose and densities of 200 kg/m^3 and 300 kg/m^3. The reaction rates of lower density fuel are higher and less spaced out compared to higher density fuel. This means more time is required for fuel to be converted in to char and ash as observed in the mass fraction section of the Fig 3.8. This dependence come from the fact that increased density of the fuel leads to more mass in the given volume that needs to be converted in to char and ash which results into slower shrinkage of fuel giving slower access to oxygen to the formed char.

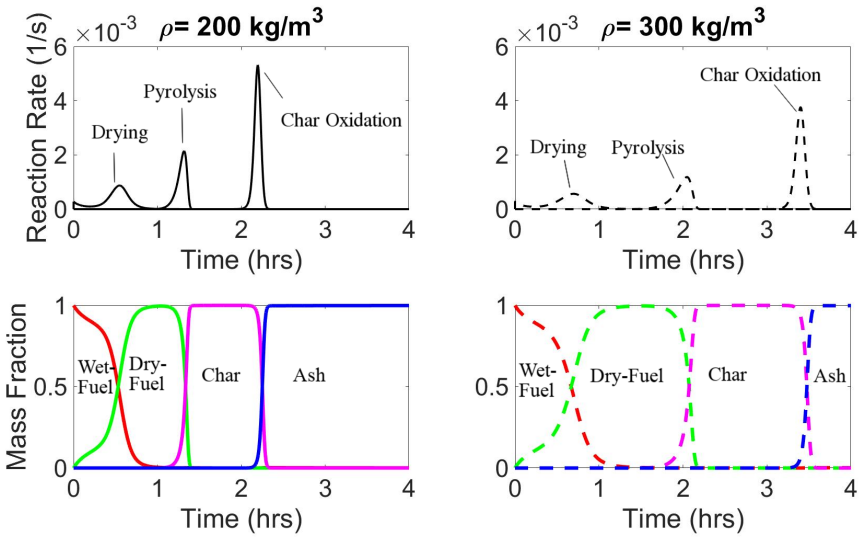

Figure 3.8: Reaction rates and mass fraction of 100 % cellulose with density 200 kg/m^3 and 300 kg/m^3 where red, green, pink, and blue line shows the mass fraction of wet fuel, dry fuel, char, and ash respectively

Across all fuel compositions, the propagation speed decreases by a factor of 0.5 when the density of fuel increases from 200 kg/m^3 to 400 kg/m^3 i.e. by a factor of 2. Huang and Rein indicated an inverse relation between oxygen concentration and density [13]. To further examine the dependence of oxygen concentration, I increase the

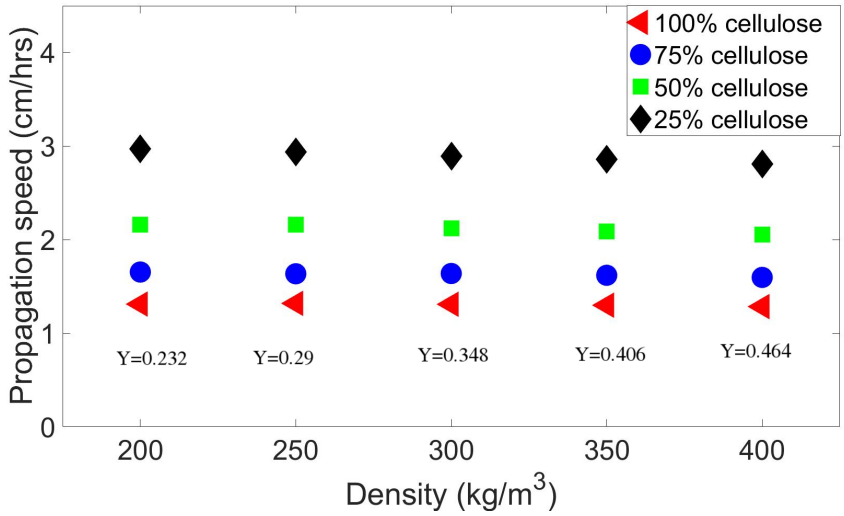

Figure 3.9: Propagation speed when oxygen availability is linearly increased with density where the value of Y indicates the value of mass fraction of oxygen used for the respective density.

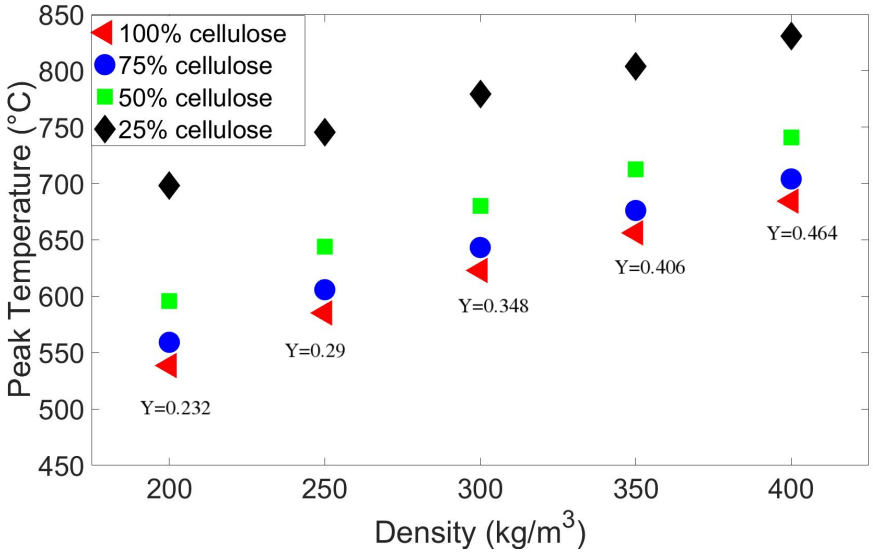

Figure 3.10: Peak temperatures when oxygen availability is linearly increased with density where the value of Y indicates the value of mass fraction of oxygen used for the respective density.

oxygen concentration by the same factor as density. The oxygen supply was increased by increasing the mass fraction of diffusing oxygen. For example if the density increases by a factor of 1.5, from 200 kg/m^3 to 300 kg/m^3, then oxygen mass fraction was set to 0.348 for 300 kg/m^3. This was done for all the densities and fuel composition shown in Fig. 3.6. Figure 3.9, shows that when mass fraction of oxygen (Y_{O_2}) increases by the same factor as density (ρ) the propagation velocities (S) becomes constant, confirming that $S \propto Y_{O_2}/\rho$ relationship poised by Huang and Rein [13]. Similar analysis of increasing oxygen supply with density was also performed with peak temperatures. Resulted obtained from that study is shown in Figure 3.10. In Fig. 3.10, peak temperatures increases with increase in the oxygen supply since peak temperature is less sensitive to density as previously shown in Fig. 3.2.

To understand how propagation speed and peak temperatures quantitatively scales with all the controlling variables. Data from Fig. 3.2, Fig. 3.6, Fig. 3.9, and Fig. 3.10 is modeled by performing linear regression using MATLAB inbuilt function regress where the independent variables includes mass fraction of cellulose ($Y_{cellulose}$), density (ρ), and oxygen concentration (Y_{O2}) and dependent variable is velocity (S) and peak temperature (T) the equation is given below:

$$S = 2545.29 \times \frac{Y_{O2}^{1.0638}}{\rho^{1.1256} \times Y_{cellulose}^{0.5755}} \tag{3.32}$$

$$T = 1775.256 \times \frac{Y_{O2}^{0.4208}}{\rho^{0.1074} \times Y_{cellulose}^{0.1550}} \tag{3.33}$$

The goodness of fit i.e. R^2 value for both this equation is approximately around 0.99. In Equation 3.32, the density of fuel (ρ) and mass fraction fraction of oxygen (Y_{O_2}) are both raised to values 1.1295 and 1.0735 which are both close to 1 establishing the near $S \propto Y_{O_2}/\rho$ as discussed earlier. Peak temperature as shown in Equation 3.33 is least sensitive to density and most sensitive to oxygen supply.

3.3.3 Effect of moisture content on propagation speed

Now I look into how moisture content affects the propagation speed and peak temperatures of smoldering combustion when fuel expands and when fuel does not expand on addition of water. This study is done since most of the woody fuel has not reported any expansion on addition of water but some fuel like peat has reported an expansion [13].

Figure 3.11 shows the effect of adding moisture content on smoldering propagation speed and peak temperatures in an expanding and non-expanding fuel. Note that moisture content is increased from 10% to 70% with an increment of 20% on 100% cellulose. In Fig. 3.11 for both, with expansion and without expansion the temperature drops as moisture content is added to the fuel however propagation speed shows opposite trends.

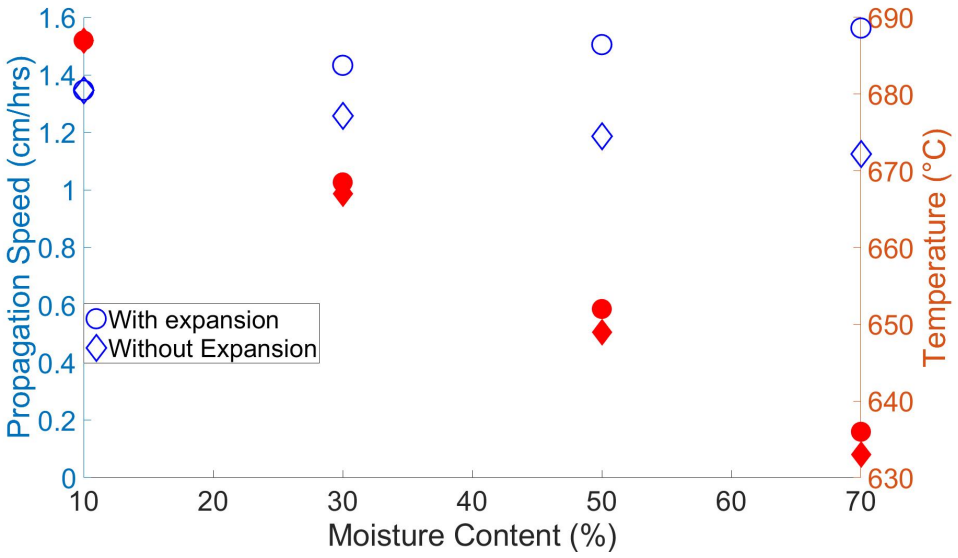

Figure 3.11: Effect of moisture content on propagation speed and mean peak temperatures with and with out expansion for 100% cellulose where the empty symbols indicate propagation speed and filled symbols indicate temperatures.

When there is no expansion involved, i.e., all the water added to the fuel sample occupies the pores, the propagation speed decreases with increasing in moisture content. In contrast when the fuel expands, i.e., addition of water increases the total volume of the fuel, then propagation speed increases with moisture content. In case without expansion when water is added to the fuel the physical parameters that increase includes thermal

conductivity, heat capacity and wet fuel bulk density. In addition when moisture content of the fuel increases, the drying involved becomes more endothermic which increases the heat of reaction.

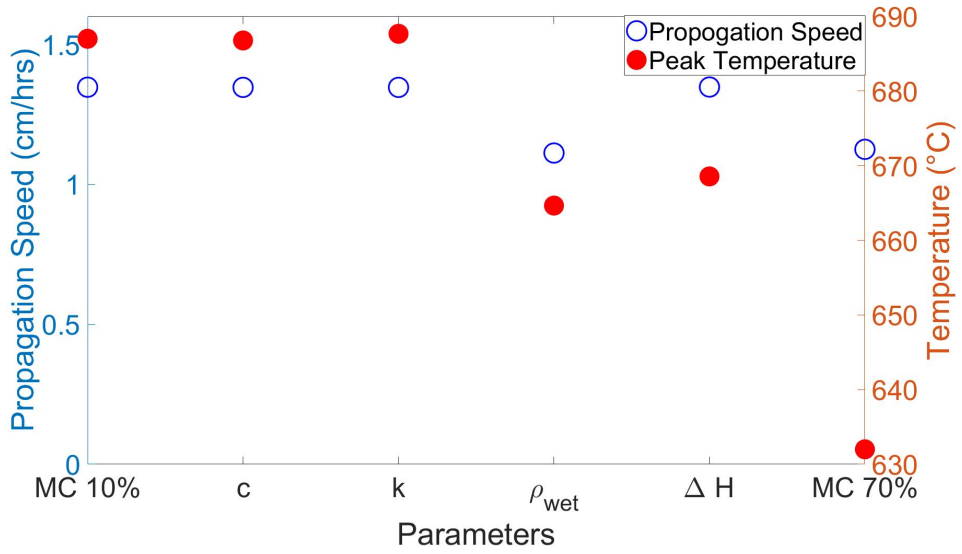

Figure 3.12: Parameter analysis for moisture content without expansion. Each parameter (c, k, ρ_{wet}, and ΔH) was changed to its value for 70% moisture content while holding all other properties to their values at 10%. The fully 10% and 70% MC cases are shown at the far left and right for comparison.

To examine which parameters contribute the most in reduction of speed and temperatures, I perform a parameter analysis as shown in Figure 3.12. Each parameter that changes on addition of moisture content was set equal to the values used for moisture content 70% keeping all the parameters constant. From Fig. 3.12 I see that thermal conductivity and heat capacity minimally affects both the propagation speed and mean peak temperatures. Increase in the wet bulk density is the main reason for the drop in the propagation speed. Where as both increase in the wet bulk density and heat of reaction contributes to the drop in temperatures. When I increase the wet fuel bulk density it means that more mass of fuel needs to be dried by the smoldering front in a given volume which results into drop in temperature and propagation speed. When the reaction becomes more endothermic, more heat is required by the char oxidation

reactions to dry the fuel, which reduces peak temperature that are attained.

In cases where the fuel expands, the increase in speed either could be due to the expansion of the fuel, which results into lower density fuel, or increase in the thermal conductivity of the fuel. I found that changing only the thermal conductivity of the fuel negligibly affects the propagation speed and temperatures, while including expansion alone increases the propagation speed. When a fuel expands the overall density of the fuel decreases. As observed in Fig 3.6, when the density of the fuel drops the propagation speed increases. So, in this case, propagation speed is more influenced by the overall reduction in density than increase in the wet mass of the fuel, which increases the propagation speed. Huang and Rein found similar results for peat [13]. The temperature reduction in this case comes from the increasing mass of wet fuel and increasing endothermicity, similar to fuels without expansion. The temperature trends are similar in both cases, since, as Eq. 3.33 shows, temperature is less sensitive to density and thus expansion.

3.3.4 Effect of changing composition on critical moisture content

Critical moisture content of ignition is the moisture content above which fuel will not ignite for a given boundary condition; critical moisture content of extinction is the moisture content above which an established smoldering front does not propagate for given upstream, downstream, and boundary conditions. In this section I will examine whether critical moisture content changes with fuel composition. For this study I hold density of the fuel at $200\,\mathrm{kg/m^3}$. A heat flux at $25\,\mathrm{kW/m^2}$ for the first 20 min and then removed to ignite the sample. Simulations were run only at compositions 100%, 75%, 50%, and 25% cellulose and the moisture content is increased by an intervals of 10%. To measure the critical moisture content of ignition, I assume a uniform moisture content throughout the fuel sample. To measure the critical moisture content of extinction I modelled the top 5 cm of the domain with 10% moisture content to establish a self sustained smoldering front followed by a wet layer of 2 cm whose moisture content was systematically increased to determine the critical moisture content of extinction with the remaining 3 cm at 10% moisture content fuel.

Now I examine whether fuel composition affects the critical moisture content, shown in Figure 3.13. In Fig. 3.13, the line joining the composition with the moisture content is the highest moisture content where I observe ignition or propagation. In other words, all

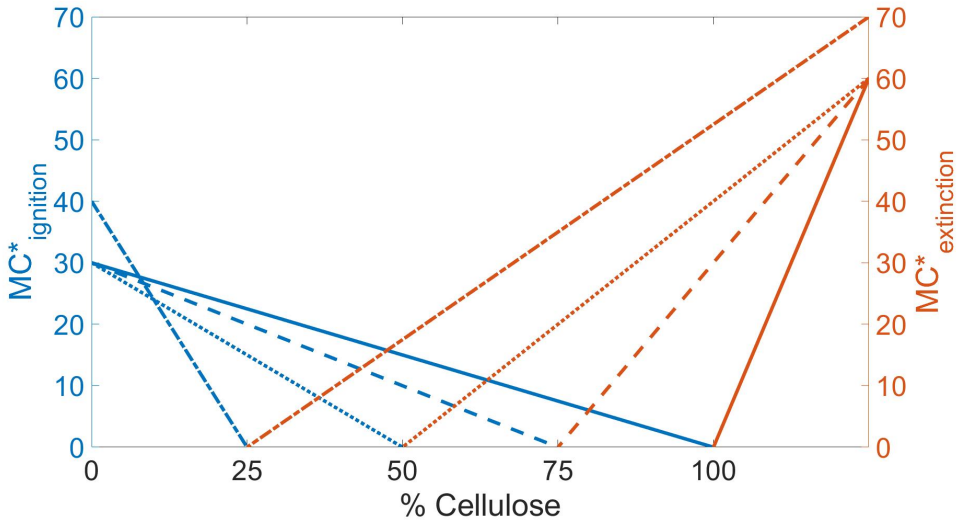

Figure 3.13: Critical moisture content of ignition and extinction for different fuel compositions.

the moisture content values below the line permits a self-sustained smoldering. The lines on the right connect to the highest content allowable before smoldering extinguishes. For all the compositions critical moisture content of ignition is always lower than the critical moisture content of extinction. Neither critical moisture contents are sensitive to fuel composition until the mixture contains 75% hemicellulose where both critical moisture content of ignition and extinction both increased by 10%. As previously shown in Fig. 3.2, adding hemicellulose to the fuel increases the mean peak temperature of the sample. At this composition, the fuel samples become hot enough to sustain smoldering combustion even at 10% higher moisture content.

Figure 3.14 shows the temperature profiles at different depths for fuel samples when the moisture content of wet layers is 60% and when it is 70%. Note that in case when the moisture content of wet layer is 60% smoldering combustion propagates through the wet layer but when the moisture content is 70% smoldering combustion extinguishes. At depth 2 cm the peak for both the case is same. However, as the smoldering front progress deeper, the difference in the moisture content downstream starts affecting the temperatures from 3 cm onward. At a depth 4 cm the temperature for the 70% moisture content case drops below the point where smoldering cant self-sustain and it extinguishes. On the other

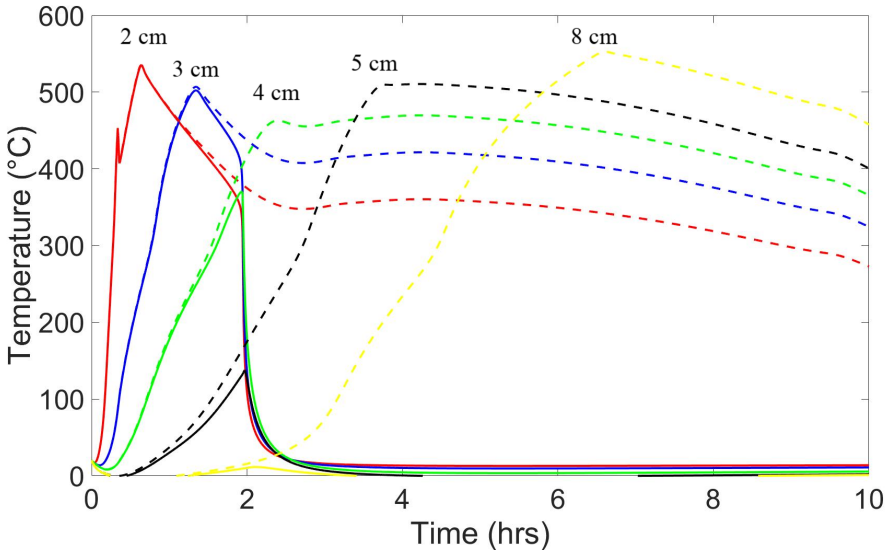

Figure 3.14: Temperature profiles of 100% cellulose with moisture content of wet layer 60% shown by dashed line and 70% shown by solid line at various depth

hand, the sample 60% moisture content has a peak temperature just below 500 °C at 4 cm which high enough to sustain smoldering. The biggest drop in the temperature in seen approximately place 1 cm above from the point the wet layer with moisture content 60% starts since till the point the smoldering wave reaches the wet layer, the layer has already dried.

3.4 Conclusion

In this chapter, I updated a one-dimensional computational model using the open-source software Gpyro. The model successfully predicts results from experiments at four fuel densities and compositions. The model successfully ignites at densities less than 200 kg/m^3, unlike the previous model [45]. A sensitivity analysis was performed using the model to understand the effect of density and fuel composition on smoldering combustion. The two parameters of interest were smoldering propagation speed and mean peak temperature.

As the density of the fuel increases, the mean propagation speed drops. This is caused by the increase in the amount of fuel that needs to be converted to ash, which

slows the fuel shrinkage and thus access to oxygen. In contrast, smoldering propagation speed increases with growing hemicellulose content in the fuel, due to earlier pyrolysis of hemicellulose compared with cellulose. Mean peak temperature also increases with additional hemicellulose content, caused by the formation of ash with lower thermal conductivity. Like smoldering propagation speed, mean peak temperature decreases with increasing density, due to increasing thermal conductivity of the fuel.

When moisture content is added and the fuel is allowed to expand, the propagation speed increases due to the reduction in density If the fuel does not expand with the addition of water, propagation speed drops primarily due to the increase in wet bulk density. In both cases, additional moisture content reduces the mean peak temperature slightly. Fuel composition affects critical moisture content of ignition and extinction if hemicellulose is the major constituent, due to the increase in temperature on addition of hemicellulose.

Supplementary material

The appendix contains the kinetic parameters used in the model (App. C), a grid convergence study (App. D), and the impact of reducing depth interval on propagation speed (App. E).

Chapter 4: Summary and conclusion

4.1 Summary

In this thesis, I first developed an initial one-dimensional transient computational model to simulate downward propagation of smoldering combustion in cellulose and hemicellulose mixtures. The model was developed using the open-source software Gpyro, representing smoldering kinetics using a global reaction scheme based on a model developed by Huang and Rein [1]. Physical properties were either measured or obtained from the literature. An initial analysis observed global trends in smoldering propagation and peak temperatures with varying density, fuel composition, and moisture content. I then updated the model and validated it against an improved experimental configuration, and used this for a more in-depth analysis. To examine the effects of varying density and fuel composition on smoldering combustion, I varied the density of the fuel from 200 $\mathrm{kg/m^3}$ to 400 $\mathrm{kg/m^3}$ and fuel composition from 100% to 50% in increments of 25% cellulose. Then, the effects of moisture content on smoldering combustion were examined by varying moisture content from 10% to 70% in cellulose, both with and without fuel expansion with the addition of water. Finally, I examined the effects of varying fuel composition on the critical moisture contents of ignition and extinction.

4.2 Conclusions

In this section I list the main conclusions and outcomes of my thesis:

- The model successfully predicts propagation speed and temperature trends observed in experiments, with average errors of 3.3% and 6.4% in mean peak temperature and propagation speed, respectively.
- Propagation speed decreases with increasing density for all fuel compositions. This happens because increasing the bulk density in a given volume means more mass of fuel needs to be converted to char and ash, resulting in slower shrinkage of the fuel, slowing access to oxygen and reducing propagation speed.

- Propagation speed increases with increasing hemicellulose content, because hemicellulose pyrolyzes faster compared with cellulose, more-quickly shrinking the fuel and giving faster access to oxygen, ultimately increasing the propagation speed.
- Peak temperatures decrease with increasing density. This is because as the density increases, the volume occupied by the solid increases, which increases the solid thermal conductivity of all the condensed-phase species, which finally results in a drop in temperature.
- Peak temperatures increase with hemicellulose content, because lower-thermal-conductivity ash forms at the top when hemicellulose is added, due to the lower pore size of hemicellulose compared with cellulose.
- For a given fuel composition, propagation speed is directly proportional to oxygen supply and inversely proportional to bulk density.
- I developed a semi-empirical correlation that gives an average spread rate and average propagation speed.
- Propagation speed decreases with increasing moisture content if the fuel does not expand with the addition of water. This is primarily caused by the increased density (leading to a larger amount of wet fuel to dry).
- Propagation speed increases with increasing moisture content if the fuel expands (like peat) with the addition of water. This is because the expansion effect reduces the overall bulk density of the fuel, which increases propagation speed.
- The critical moisture content of ignition is smaller than the critical moisture of extinction for all fuel compositions.
- Fuel composition affects critical moisture content: fuel mixtures dominated by hemicellulose have higher critical moisture content of ignition and extinction. Increasing hemicellulose content increases in the peak temperatures of the fuel, which helps the smoldering front maintain temperatures high enough to sustain smoldering combustion at higher moisture contents.

4.3 Future work

Future work should study mixtures with lignin, which is the third major of woody fuels and biomass along with cellulose and hemicellulose. Thus, the model developed in this work should be extended to include lignin, and its contribution to pyrolysis and combustion needs to be examined. Real fuels also include inorganic content, which acts as a heat sink, and their effects should also be considered. Capturing all of these effects and accurate interactions between the complex components of biomass—including those beyond cellulose, hemicellulose, and lignin—may require a more detailed chemical model with additional species and reactions. In addition, since smoldering fronts in reality propagate in multiple dimensions, studying the structure of the front in more detail requires extending this analysis to two- and eventually three-dimensional simulations.

Once all the major fuel constituents are incorporated in the model, it should be examined whether smoldering characteristics of any real fuel can be predicted by matching their fuel composition, physical properties, moisture content, and inorganic content. This could lead to generalizable predictive models usable in both large-scale fire simulations and by fire and land managers for helping make critical decisions.

Bibliography

[1] X Huang and G Rein, "Thermochemical conversion of biomass in smouldering combustion across scales: The roles of heterogeneous kinetics, oxygen and transport phenomena," Bioresource Technology **207**, 409–421 (2016) 10.1016/j.biortech.2016.01.027.

[2] T Kashiwagi and H Nambu, "Global kinetic constants for thermal oxidative degradation of a cellulosic paper," Combustion and Flame **88**, 345–368 (1992) 10.1016/0010-2180(92)90039-R.

[3] R Moriana, Y Zhang, P Mischnick, J Li, and M Ek, "Thermal degradation behavior and kinetic analysis of spruce glucomannan and its methylated derivatives," Carbohydrate Polymers **106**, 60–70 (2014) 10.1016/j.carbpol.2014.01.086.

[4] MJ Power, J Marlon, N Ortiz, PJ Bartlein, SP Harrison, FE Mayle, A Ballouche, RHW Bradshaw, C Carcaillet, C Cordova, S Mooney, PI Moreno, IC Prentice, K Thonicke, W Tinner, C Whitlock, Y Zhang, Y Zhao, AA Ali, RS Anderson, R Beer, H Behling, C Briles, KJ Brown, A Brunelle, M Bush, P Camill, GQ Chu, J Clark, D Colombaroli, S Connor, AL Daniau, M Daniels, J Dodson, E Doughty, ME Edwards, W Finsinger, D Foster, J Frechette, MJ Gaillard, DG Gavin, E Gobet, S Haberle, DJ Hallett, P Higuera, G Hope, S Horn, J Inoue, P Kaltenrieder, L Kennedy, ZC Kong, C Larsen, CJ Long, J Lynch, EA Lynch, M McGlone, S Meeks, S Mensing, G Meyer, T Minckley, J Mohr, DM Nelson, J New, R Newnham, R Noti, W Oswald, J Pierce, PJH Richard, C Rowe, MF Sanchez Goñi, BN Shuman, H Takahara, J Toney, C Turney, DH Urrego-Sanchez, C Umbanhowar, M Vandergoes, B Vanniere, E Vescovi, M Walsh, X Wang, N Williams, J Wilmshurst, and JH Zhang, "Changes in fire regimes since the last glacial maximum: an assessment based on a global synthesis and analysis of charcoal data," Climate Dynamics **30**, 887–907 (2008) 10.1007/s00382-007-0334-x.

[5] M Koerth-Baker, "Wildfires in the U.S. are getting bigger," FiveThirtyEight (2018).

[6] M Flannigan, M Krawchuk, M Wotton, and L Johnston, "Implications of changing climate for global wildland fire," International Journal of Wildland Fire **18**, 483–507 (2009) 10.1071/WF08187.

[7] MR Raupach, G Marland, P Ciais, C Le Quéré, JG Canadell, G Klepper, and CB Field, "Global and regional drivers of accelerating CO_2 emissions," Proceedings of the National Academy of Sciences **104**, 10288–10293 (2007) 10.1073/pnas.0700609104.

[8] DE Ward and CC Hardy, "Smoke emissions from wildland fires," Environment International **17**, 117–134 (1991) 10.1016/0160-4120(91)90095-8.

[9] G Rein, "Smouldering Combustion," in *SFPE Handbook of Fire Protection Engineering*, edited by Hurley M. J. et al. (Springer, New York, NY, 2016) Chap. 19, pp. 581–603, 10.1007/978-1-4939-2565-0_19.

[10] G Rein, "Smouldering Combustion Phenomena in Science and Technology," International Review of Chemical Engineering **1**, 3–18 (2009).

[11] A Anca-Couce, N Zobel, A Berger, and F Behrendt, "Smouldering of pine wood: Kinetics and reaction heats," Combustion and Flame **159**, 1708–1719 (2012) 10.1016/j.combustflame.2011.11.015.

[12] BC Hagen, V Frette, G Kleppe, and BJ Arntzen, "Onset of smoldering in cotton: effects of density," Fire Safety Journal **46**, 73–80 (2011) 10.1016/j.firesaf.2010.09.001.

[13] X Huang and G Rein, "Downward spread of smouldering peat fire: the role of moisture, density and oxygen supply," International Journal of Wildland Fire **26**, 907–918 (2017) 10.1071/WF16198.

[14] X Huang, G Rein, and H Chen, "Computational smoldering combustion: Predicting the roles of moisture and inert contents in peat wildfires," Proceedings of the Combustion Institute **35**, 2673–2681 (2015) 10.1016/j.proci.2014.05.048.

[15] SE Page, F Siegert, JO Rieley, HDV Boehm, A Jaya, and S Limin, "The amount of carbon released from peat and forest fires in indonesia during 1997," Nature **420**, 61–65 (2002).

[16] TJ Ohlemiller, "Smoldering combustion," in *Sfpe handbook of fire protection engineering*, edited by PJ Di Nenno, D Drysdale, CL Beyler, and WD Walton, 3rd ed. (NFPA, Quincy, 2002) Chap. 9, pp. 200–210.

[17] D Drysdale, *An introduction to fire dynamics*, 3rd ed. (Wiley, UK, 2011).

[18] K Miyanshi, "Duff Composition," in *Forest Fires: Behavior and Ecological Effects*, edited by EA Johnson and K Miyanishi (Academic Press, 2001), pp. 435–475, 10.1016/B978-012386660-8/50015-5.

[19] A Gani and I Naruse, "Effect of cellulose and lignin content on pyrolysis and combustion characteristics for several types of biomass," Renewable Energy **32**, 649–661 (2007) 10.1016/j.renene.2006.02.017.

[20] DA Cowan, BD Smucker, and DL Blunck, "Sensitivity of smoldering combustion to cellulose and hemicellulose content," in 10th us combustion meeting (2017).

[21] C Lautenberger and C Fernandez-Pello, "Generalized pyrolysis model for combustible solids," Fire Safety Journal **44**, 819–839 (2009) 10.1016/j.firesaf.2009.03.011.

[22] C Lautenberger, *Gpyro v0.700*, http://reaxengineering.com/trac/gpyro, 2009.

[23] X Huang, Personal communication, 25 March 2017, 2017.

[24] C-Therm Technology, *Thermal Physical Properties Reference Library: Part II (L–R)*, http://ctherm.com/products/tci_thermal_conductivity/helpful_links_tools/thermal_physical_properties_conductivity_effusivity_heat_capacity_density2/, Accessed: 2017-08-29, 2017.

[25] R Aseeva, B Serkov, and A Sivenkov, *Fire behavior and fire protection in timber buildings*, Springer Series in Wood Science (Springer, Dordrecht, 2014).

[26] EE Thybring, "Explaining the heat capacity of wood constituents by molecular vibrations," Journal of Materials Science **49**, 1317–1327 (2014) 10.1007/s10853-013-7815-6.

[27] J Eitelberger and K Hofstetter, "Prediction of transport properties of wood below the fiber saturation point - A multiscale homogenization approach and its experimental validation. Part I: Thermal conductivity," Composites Science and Technology **71**, 134–144 (2011) 10.1016/j.compscitech.2010.11.007.

[28] RT Jacobsen, EW Lemmon, SG Penoncello, Z Shan, and NT Wright, "Thermophysical properties of fluids and materials," in *Heat transfer handbook*, Vol. 1 (John Wiley & Sons, 2003) Chap. 2, pp. 43–160.

[29] F Yu, G Wei, X Zhang, and K Chen, "Two effective thermal conductivity models for porous media with hollow spherical agglomerates," International Journal of Thermophysics **27**, 293–303 (2006) 10.1007/s10765-006-0032-7.

[30] B Punmia and AK Jain, *Soil mechanics and foundations* (Laxmi Publication Pvt Limited, 2005).

[31] Sigma-Aldrich, *α-Cellulose*, http://www.sigmaaldrich.com/catalog/product/sigma/c8002?lang=en&region=US, Accessed: 2017-08-29, 2017.

[32] M Schure, PA Soltys, DFS Natusch, and T Mauney, "Surface area and porosity of coal fly ash," Environmental Science & Technology **19**, 82–86 (1985) 10.1021/es00131a009.

[33] X Huang and G Rein, "Smouldering combustion of peat in wildfires: Inverse modelling of the drying and the thermal and oxidative decomposition kinetics," Combustion and Flame **161**, 1633–1644 (2014) 10.1016/j.combustflame.2013.12.013.

[34] C Huggett, "Estimation of rate of heat release by means of oxygen consumption measurements," Fire and Materials **4**, 61–65 (1980) 10.1002/fam.810040202.

[35] H Yang, "Characteristics of hemicellulose, cellulose and lignin pyrolysis," Fuel **86**, 1781–1788 (2007) 10.1016/j.fuel.2006.12.013.

[36] Y Liu, J Stanturf, and S Goodrick, "Trends in global wildfire potential in a changing climate," Forest Ecology and Management **259**, 685–697 (2010) 10.1016/j.foreco.2009.09.002.

[37] AC Watts and LN Kobziar, "Smoldering combustion and ground fires: ecological effects and multi-scale significance," Fire Ecology **9**, 124–132 (2013) 10.4996/fireecology.0901124.

[38] R Hartford and W Frandsen, "When it's hot, it's hot... or maybe it's not! (surface flaming may not portend extensive soil heating)," International Journal of Wildland Fire **2**, 139–144 (1992) 10.1071/WF9920139.

[39] G Rein, "Smouldering fires and natural fuels," in *Fire phenomena and the earth system* (Wiley-Blackwell, 2013) Chap. 2, pp. 15–33, 10.1002/9781118529539.ch2.

[40] H Yang, R Yan, H Chen, DH Lee, and C Zheng, "Characteristics of hemicellulose, cellulose and lignin pyrolysis," Fuel **86**, 1781–1788 (2007) 10.1016/j.fuel.2006.12.013.

[41] B Cagnon, X Py, A Guillot, F Stoeckli, and G Chambat, "Contributions of hemicellulose, cellulose and lignin to the mass and the porous properties of chars and steam activated carbons from various lignocellulosic precursors," Bioresource Technology **100**, 292–298 (2009) 10.1016/j.biortech.2008.06.009.

[42] BD Smucker, TC Mulky, DA Cowan, KE Niemeyer, and DL Blunck, "Effects of fuel content and density on the smoldering characteristics of cellulose and hemicellulose," Proceedings of the Combustion Institute (2019) 10.1016/j.proci.2018.07.047.

[43] E C. Garlough and C Keyes, "Influences of moisture content, mineral content and bulk density on smouldering combustion of ponderosa pine duff mounds," International Journal of Wildland Fire **20**, 589–596 (2011) 10.1071/WF10048.

[44] X Huang and G Rein, "Computational study of critical moisture and depth of burn in peat fires," International Journal of Wildland Fire **24**, 798–808 (2015) 10.1071/WF14178.

[45] TC Mulky and KE Niemeyer, Proceedings of the Combustion Institute, in press (2019) 10.1016/j.proci.2018.06.164.

[46] National Organic Standard Board Technical Advisory Panel, *Cellulose Processing*, https://www.ams.usda.gov/sites/default/files/media/Cellulose%20TR%202001, Accessed: 2017-08-29, 2017.

[47] parchem, *Glucomannan*, https://www.parchem.com/chemical-supplier-distributor/Glucomannan-007456.aspx, Accessed: 2017-08-29, 2017.

[48] BD Smucker, DA Cowan, and DL Blunck, Personal communication, 15 February 2018, 2018.

APPENDICES

Appendix A: Details about experimental data in Chapter 2

The experiments were conducted on four cellulose and hemicellulose mixtures with varying density and compositions [48]. The cellulose content was varied from 100% to 25% by mass with a decrement of 25% the remaining portion being hemicellulose where the density of the fuels were 188.75 $\mathrm{kg/m^3}$, 237.14 $\mathrm{kg/m^3}$, 364.28 $\mathrm{kg/m^3}$, and 527.71 $\mathrm{kg/m^3}$, respectively. The fuel samples were held in a rector box with the following dimensions: $20 \times 20 \times 10$ cm. The reactor box was made from fiberboard. The top surface was open to the atmosphere. The cellulose used in the experiments was α-cellulose purchased from Sigma-Aldrich (CAS no: 9004-34-6) and hemicellulose used in the experiments was glucomannon purchased from Nutricost. The fuel was ignited using a 20 W cartridge heater with a diameter of 64 mm. The cartridge heater was placed at the center of the reactor box. Type-K thermocouples were placed at 0, 2.5, 5, and 7.5 cm from the top surface.

Appendix B: Reaction parameters for Chapter 2

$$\text{Cellulose} \cdot v_{w,dr}\text{H}_2\text{O} \longrightarrow \text{Cellulose} + v_{w,dr}\text{H}_2\text{O}\,(\text{g}) \tag{B.1}$$

$$\text{Cellulose} \longrightarrow v_{\alpha,cp}\alpha\text{−Char}_c + v_{g,cp}\text{Gas} \tag{B.2}$$

$$\text{Cellulose} + v_{O_2,co}\text{O}_2 \longrightarrow v_{\beta,co}\beta\text{−Char}_c + v_{g,co}\text{Gas} \tag{B.3}$$

$$\alpha\text{-Char}_c + v_{O_2,c\alpha o}\,\text{O}_2 \longrightarrow v_{a,c\alpha o}\text{Ash}_c + v_{g,c\alpha o}\text{Gas} \tag{B.4}$$

$$\beta\text{-Char}_c + v_{O_2,c\beta o}\text{O}_2 \longrightarrow v_{a,c\beta o}\text{Ash}_c + v_{g,c\beta o}\text{Gas} \tag{B.5}$$

$$\text{Hemicellulose} \cdot v_{w,dr}\text{H}_2\text{O} \longrightarrow \text{Hemicellulose} + v_{w,dr}\text{H}_2\text{O}\,(\text{g}) \tag{B.6}$$

$$\text{Hemicellulose} \longrightarrow v_{\alpha,hp}\alpha\text{−Char}_h + v_{g,hp}\text{Gas} \tag{B.7}$$

$$\text{Hemicellulose} + v_{O_2,ho}\text{O}_2 \longrightarrow v_{\beta,ho}\beta\text{−Char}_h + v_{g,ho}\text{Gas} \tag{B.8}$$

$$\alpha\text{-Char}_h + v_{O_2,h\alpha o}\text{O}_2 \longrightarrow v_{a,h\alpha o}\text{Ash}_h + v_{g,h\alpha o}\text{Gas} \tag{B.9}$$

$$\beta\text{-Char}_h + v_{O_2,h\beta o}\text{O}_2 \longrightarrow v_{a,h\beta o}\text{Ash}_h + v_{g,h\beta o}\text{Gas} \tag{B.10}$$

where v is the stoichiometric coefficient; α and β indicate char produced from fuel pyrolysis and fuel oxidation reactions, respectively; and subscripts w, g, O_2, a, c, h, dr, o, p, αo, βo are water, gas, oxygen, ash, cellulose, hemicellulose, drying, oxidation, pyrolysis, α-char oxidation, and β-char oxidation, respectively.

Table B.1 lists the reaction parameters for the chemical kinetic schemes used in the simulation, obtained from Huang and Rein [1].

Table B.1: Kinetic parameters for cellulose and hemicellulose models from Huang and Rein [1–3].

Reaction number	Reaction	$\log Z$ $\log \mathrm{s}^{-1}$	E kJ/mol	ΔH MJ/kg	n –	n_{O_2} –	v –	v_{O_2} –
		Cellulose						
(1)	Drying	8.12	67.8	2.26	2.37	–	0	0
(2)	Pyrolysis	11.7	156	0.5	1	–	0.24	0
(3)	Oxidation	24.2	278	-28.2	1.73	0.74	0.21	1.81
(4)	β-char oxidation	7.64	120	-28.8	1.25	0.89	0.03	2.22
(5)	α-char oxidation	12.2	177	-27.8	0.93	0.52	0.03	2.22
		Hemicellulose						
Reaction number	Reaction	$\log Z$ $\log \mathrm{s}^{-1}$	E kJ/mol	ΔH MJ/kg	n –	n_{O_2} –	v –	v_{O_2} –
(6)	Drying	8.12	67.8	2.26	2.37	–	0	0
(7)	Pyrolysis	6.95	93.8	0.5	0.98	–	0.265	0
(8)	Oxidation	20.2	294	-20.9	0.47	0.11	0.265	1.683
(9)	β-char oxidation	7.64	120	-28.8	1.25	0.89	0.064	2.1432
(10)	α-char oxidation	12.2	177	-27.8	0.93	0.52	0.064	2.1432

Appendix C: Reaction parameters for Chapter 3

Table C.1: Kinetic parameters for cellulose and hemicellulose models from Huang and Rein [1, 2].

Reaction number	Reaction	$\log Z$ $\log \mathrm{s}^{-1}$	E kJ/mol	ΔH MJ/kg	n –	n_{O_2} –	v –	v_{O_2} –
		Cellulose						
(1)	Drying	8.12	67.8	2.26	2.37	–	0	0
(2)	Pyrolysis	11.7	156	0.5	1	–	0.24	0
(3)	Oxidation	24.2	278	-28.2	1.73	0.74	0.21	1.81
(4)	β-char oxidation	7.64	120	-28.8	1.25	0.89	0.03	2.22
(5)	α-char oxidation	12.2	177	-27.8	0.93	0.52	0.03	2.22
		Hemicellulose						
Reaction number	Reaction	$\log Z$ $\log \mathrm{s}^{-1}$	E kJ/mol	ΔH MJ/kg	n –	n_{O_2} –	v –	v_{O_2} –
(6)	Drying	8.12	67.8	2.26	2.37	–	0	0
(7)	Pyrolysis	6.95	93.8	0.5	0.98	–	0.16	0
(8)	Oxidation	20.2	294	-20.9	0.47	0.11	0.30	1.60
(9)	β-char oxidation	7.64	120	-28.8	1.25	0.89	0.04	2.1985
(10)	α-char oxidation	12.2	177	-27.8	0.93	0.52	0.08	2.1069

Appendix D: Grid convergence

We performed a grid convergence study, as shown in Figure D.1 for the smoldering wave propagation speed as a function of cell size. Our simulations were performed using a uniform cell size of 1×10^{-4} m, and as Fig. D.1 shows reducing the cell size further leads to negligible change in the propagation speed.

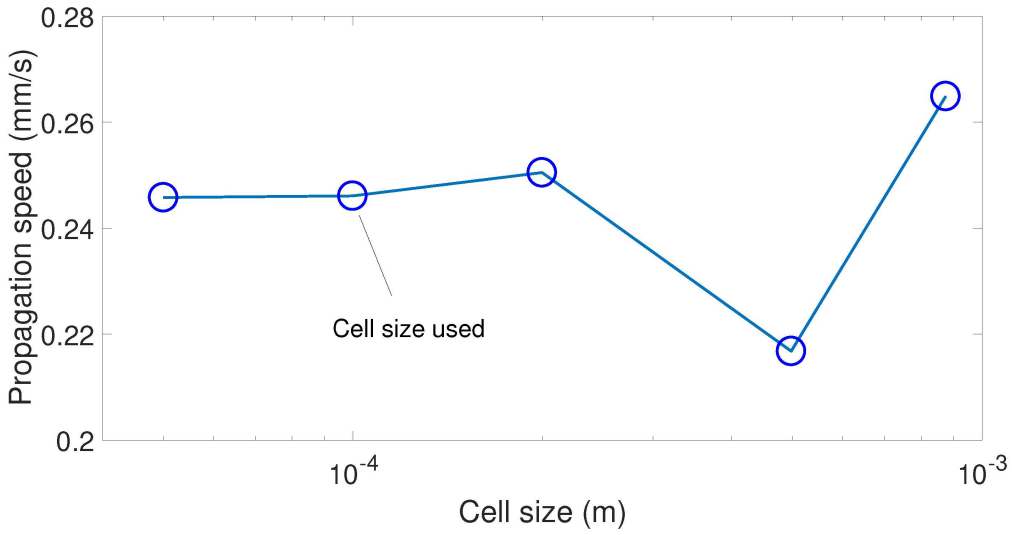

Figure D.1: Impact of refining the uniform grid size on calculated propagation speed of the smoldering wave.

Appendix E: Temperature depth interval

In this study the depth interval between temperatures to calculate propagation speed was varied to study its effects on the average propagation speed. Figure E.1 shows the results from the study. Based on the result of the study we selected depth interval of 1 cm to calculate the propagation speed since reducing it further by a factor of 2 had resulted into change in the speed less than 0.3%.

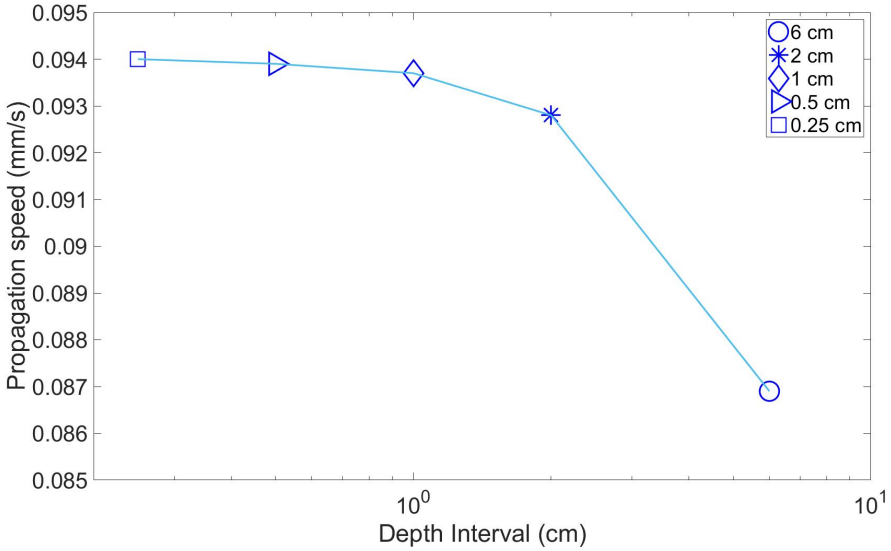

Figure E.1: Impact of changing the depth interval between temperatures on calculated propagation speed.